LBL-30942

Center for Advanced Materials

CAM

Magnetic Field-Induced Fracture Changes in Metastable Austenites at 4.2K

J.W. Chan
(Ph.D. Thesis)

June 1991

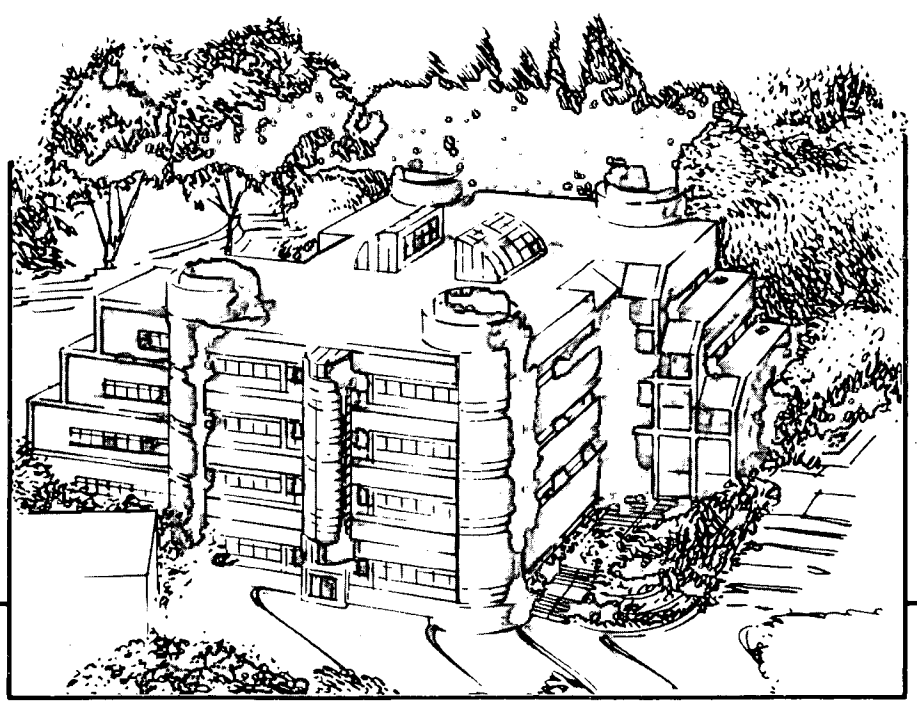

Materials and Chemical Sciences Division

Lawrence Berkeley Laboratory • University of California

ONE CYCLOTRON ROAD, BERKELEY, CA 94720 • (415) 486-4755

Prepared for the U.S. Department of Energy under Contract DE-AC03-76SF00098

| LOAN COPY |
|Circulates |
|for 4 weeks|

Bldg. 50 Library.

LBL-30942

Copy 2

DISCLAIMER

This document was prepared as an account of work sponsored by the United States Government. While this document is believed to contain correct information, neither the United States Government nor any agency thereof, nor the Regents of the University of California, nor any of their employees, makes any warranty, express or implied, or assumes any legal responsibility for the accuracy, completeness, or usefulness of any information, apparatus, product, or process disclosed, or represents that its use would not infringe privately owned rights. Reference herein to any specific commercial product, process, or service by its trade name, trademark, manufacturer, or otherwise, does not necessarily constitute or imply its endorsement, recommendation, or favoring by the United States Government or any agency thereof, or the Regents of the University of California. The views and opinions of authors expressed herein do not necessarily state or reflect those of the United States Government or any agency thereof or the Regents of the University of California.

LBL-30942

Magnetic Field-Induced Fracture Changes in Metastable Austenites at 4.2 K

J. W. Chan

Ph.D. Dissertation

Department of Materials Science and Mineral Engineering

University of California

and

Center for Advanced Materials
Materials Science Division
Lawrence Berkeley Laboratory
1 Cyclotron Road
Berkeley, CA 94720

June, 1991

This work is supported by the Director, Office of Energy Research, Office of Development and Technology, Office of Magnetic Systems, Base Technology Division of the U. S. Department of Energy under Contract No. *DE-AC03-76SF00098.*

Magnetic Field-Induced Fracture Changes in Metastable Austenites at 4.2K

by

Jin Wah Chan

ABSTRACT

Austenitic stainless steels have been used as structural alloys in high field superconducting magnets. Some of the candidate structural alloys for the next generation of magnetic confinement fusion reactors are of this type. In this application the alloys sustain high stresses in high strength magnetic fields at 4.2K. It is known that plastic deformation at low temperatures induces a martensitic transformation in some of these alloys and that the presence of a strong magnetic field enhances the transformation. If such potentially metastable alloys are selected for this application, their mechanical behavior under service conditions has to be examined closely. Work on the tensile behavior of 18-8 type stainless steels under conditions of cryogenic temperatures and high-strength magnetic fields indicates that the tensile behavior does not undergo large changes in an engineering sense. However, fatigue and fracture properties have not yet been examined closely. This work addresses the fracture behavior of 18-8 type austenitic alloys at 4.2K in an 8T magnetic field. The fracture toughness is found to change with the application of the magnetic field. The direction of the fracture toughness change is related to enhanced transformation due to the reduction in the stability of the alloy in the magnetic field. Materials of low stability decrease in toughness and materials of intermediate stability increase in toughness; fully stable alloys showed no change. Several mechanisms that contribute to the observed differences are identified. These include: formation of low toughness martensite regions, strain hardening rate increases due to the transformation, transformation toughening, magnetostatic interactions, and changes in the slip characteristics. The timing of the transformation influences the relative strength of the operative mechanisms and determines the direction and amount of fracture toughness change.

TABLE OF CONTENTS

	Acknowledgements	iii
1.	Introduction	1
	1.1 Background	2
2.	Experimental	5
	2.1 Calibration	7
	2.2 Mechanical Test Procedure	8
	2.3 Characterization	8
3.	Results	10
	3.1 Mechanical Test Results	10
	3.1.1 Tensile	10
	3.1.2 Fracture Toughness	10
	3.1.2.1 AISI 304	10
	3.1.2.2 AISI 304L	11
	3.1.2.3 Room Temperature-Rolled AISI 304L	11
	3.1.2.4 Warm-Rolled AISI 304L	11
	3.1.2.5 Cold-Rolled AISI 304L	11
	3.1.2.6 AISI 310S	12
	3.2 Characterization	12
	3.2.1 α' Distribution	12
	3.2.2 AISI 304	13
	3.2.3 AISI 304L	15
	3.2.4 Room Temperature-Worked 304L	16
	3.2.5 Warm-Rolled 304L	17
	3.2.6 Cold-Rolled 304L	17
	3.2.7 AISI 310S	18
4.	Discussion	19
	4.1 Magnetostatic Effects	21
	4.2 Crack Tip Shielding Effects	22
	4.3 Strain Hardening Rate Effects	26
	4.4 Crack Deflection	28
	4.5 Fracture Micromode Effects	29
5.	Conclusions	36
6.	Suggested Future Work	37
7.	References	38

ACKNOWLEDGEMENTS

I want to thank my parents for their support of all the activities that I have undertaken through the years leading to this work. I also want to express my appreciation for the patience and support that my advisor, Prof. J. W. Morris, Jr., has shown during my graduate career. Thanks also to all my co-workers and former fellow students, J. Glazer, Z. Mei, D. Chu, A. Sunwoo, and P. Kramer, who have helped with various aspects of the work presented in this thesis. Special thanks to D. Tribula and T. Summers for their critical review of this thesis and for their moral support and also to J. Glazer and Z. Mei for their many stimulating discussions on aspects of this work. Thanks also to my thesis committee members, Profs. J. W. Morris, Jr., R. O. Ritchie, and D. A. Dornfeld for their review of this thesis, and to J. Fortado for her administrative support during my graduate career.

This work is supported by the Director, Office of Energy Research, Office of Fusion Energy, Development and Technology Division of the U. S. Department of Energy under Contract No. DE-AC03-76SF00098.

1. INTRODUCTION

Austenitic stainless steels have been used as structural alloys in high field superconducting magnets. Some of the candidate structural alloys for the next generation of magnetic confinement fusion reactors are of this type. In this application, the alloys sustain high stresses in high strength magnetic fields at 4.2 K. It is known that plastic deformation at low temperatures induces martensitic transformation in some of these alloys and that the presence of a strong magnetic field enhances the transformation. If the structural alloys selected for this application undergo martensitic transformation under service conditions, there may be unanticipated effects, such as changes in the tensile, fatigue, and fracture properties that can potentially degrade the performance of the device. Even if the base alloys remain austenitic under service conditions, there remains the possibility that required welds, which commonly suffer from chemical inhomogeneities because of segregation during solidification, can in some regions be metastable. This necessitates complete characterization of the mechanical behavior: tensile, fatigue, and fracture toughness properties of these metastable alloys at the anticipated operating conditions to better understand the controlling mechanisms. In addition to the engineering interest stated, there is also a more fundamental interest in that the fracture behavior of this type of alloy under a cryogenic, high-strength magnetic field environment has not been extensively studied.

The scope of this work consists of examining the changes in fracture toughness of metastable austenites at 4.2 K in an 8 T magnetic field, identifying the underlying mechanisms responsible for these changes, and determining their relative importance.

1.1 BACKGROUND

It is well known that certain austenitic steels are metastable and can undergo strain-induced martensitic transformation at cryogenic temperatures.[1,2] The martensitic transformation behavior of 18Cr-8Ni type austenitic stainless steels has been extensively characterized.[3-15] The martensite formed in these alloys is in the form of highly dislocated laths confined between $(111)_\gamma$ slip planes with the long axis of the lath roughly parallel to $[110]_\gamma$ and the plane of the laths roughly parallel to $(225)_\gamma$ [3,12] or $(259)_\gamma$ depending on the exact chemical composition.[13] These alloys are thermally stable with respect to transformation but are unstable with deformation at low temperatures. This propensity to transform is influenced by the amount of prior deformation of the austenite[3,13] and the temperature at which this prior deformation occurs.[9,12] Prior deformation above the M_d, the temperature above which deformation will not induce a transformation, of the alloy and large amounts of prior deformation inhibit the subsequent transformation while small amounts of prior deformation tend to stimulate transformation. Grain size also influences the amount of transformation; fine grain material tends to suppress growth more than large grain material.[11,16]

It is known that the presence of a high strength magnetic field during deformation can enhance both athermal and isothermal martensitic transformation in Ni, Ni-Cr, and Mn steels.[16-23] This enhancement occurs because the alignment of the magnetic moments of a material with a magnetic field lowers its thermodynamic potential in the field. The amount of free energy change is $H\Delta M$ in the presence of the applied magnetic field, H, where ΔM is the change in saturation magnetization due to the phase change. Since the ferromagnetic martensite phase has a higher magnetization than that of the austenite phase, it has a lower free energy and is favored in the field. Experiments on Fe-Ni alloys[25] examining the reverse $\alpha' \rightarrow \gamma$ transformation in magnetic fields show that the A_s temperature, when reversion to austenite begins, is raised in a magnetic field, an

observation consistent with a more stable ferromagnetic bcc phase in a magnetic field. The decrease in austenite stability in a magnetic field affects both the rate of formation of isothermal martensite[26] and the amount of athermal martensite formed at a particular temperature. The shift in transformation temperature for athermal martensite formation due to an applied field for a number of austenitic steels has been calculated to be approximately 2 K/Tesla.[28,30]

The available data on the behavior of metastable austenitic steels in magnetic fields at 4.2 K is somewhat confusing. Studies of the plastic deformation of 18Cr alloys with Ni contents varying between 8 to 25 wt% in a 3.4 T transient magnetic field show that for Ni contents below 15 wt%, there is a detectable decrease in flow strength at strains between 0.05 and 0.1.[28] In the more stable higher Ni content alloys, there is a slight increase in flow strength with a 3.4 T magnetic field. For the same alloys in a constant magnetic field, there is no detectable differences in the tensile behavior. Goldfarb et al.[32] report no detectable transformation in AISI 304 at 4.2 K with deformation in a 3.7 T constant applied field that could be attributed to the field. Reed, Arvidson, Ekin, and Schoon[33] examined the tensile behavior of AISI 304 and AISI 310 annealed and cold-drawn wires in a constant 7 T magnetic field transversely oriented to the wire axis; within experimental uncertainty, no detectable effects on the tensile behavior nor on martensite enhancement were found.

The tensile behavior[30,34,35] and the fatigue behavior[36] of 304L and 304LN, which are less stable and more stable, respectively, than 304, in higher strength fields has also been investigated in some detail. Martensite content was enhanced for 77 K and 4.2 K tensile deformation in magnetic fields from 8 T to 18 T. The flow stress was reduced at low strains and increased at intermediate strains as compared with specimens tested at the same temperatures but without the application of a magnetic field. The total elongations

for cold-worked and as-received alloys were slightly reduced in the magnetic field while annealed specimens showed greater total elongations. The change in total elongation is accompanied by slight increases in the ultimate strengths and slightly reduced uniform elongation for the cold-worked and the as-received cases, and increased uniform elongation for the annealed case. This behavior was attributed to increased martensite formation during plastic deformation in the high strength magnetic field.

The behavior in the early stage of plastic strain at low temperatures in these alloys is consistent with the Suzuki "window" mechanism,[14,15] in which α' martensite nucleation near the slip band intersections in the parent austenite facilitates the passage of one slip band through the other, thus reducing flow stress. In strong magnetic fields, the increase in α' formation enhances this behavior, resulting in a greater reduction in flow stress at low strains (≤ 0.05). At higher strains, when the defect density increases, the window mechanism becomes less important, and the increased strain hardening rate in the magnetic field is related to the increased α' formation rate and interaction between the strain fields around the α' particles and slip in the austenite matrix. The elongation changes observed are attributed to the differences in the rate of exhaustion of α' formation capacity at large strains that presumably depend on the timing of the transformation. Substantial transformation at the early stages will tend to exhaust α' formation capacity and cause the plastic deformation at later stages to occur in the decreasing volume fraction of retained austenite until early exhaustion of the strain hardening ability. Slight fatigue crack growth rate decreases are also observed by Fultz et al.[36] for 304L and 304LN at 77 K for ΔK less than 60 MPa-m$^{1/2}$. While changes in tensile and fatigue behavior due to the presence of the higher applied magnetic fields are observed, these changes in tensile and fatigue behavior are not deemed significant in an engineering sense.

However, some recent work by Fukushima et al.[37] suggests that there may be a significant decrease in the fracture toughness of AISI 304 at 4.2 K in a 9 T magnetic field. Decreases in the J_{IC} of approximately 42% were observed in the applied field. The continuum calculations of Shindo,[40-42] which predict a decrease in fracture toughness for a soft ferromagnetic material in a high-magnetic field environment, were invoked to explain this observation. Yanagi et al. reported a 10% decrease in J_{IC} at 4 K in a 10 T transverse field for an AISI 321 equivalent steel.[43] Later work by Fukushima et al.[48] showed both improvements and degradations to fracture toughness in an 8 T magnetic field, depending on the precrack conditions for the AISI 304 specimens. The available fracture toughness data for metastable alloys in a cryogenic, high-magnetic field environment is limited and the mechanisms that are involved have not been adequately examined.

From the data on the tensile behavior of metastable alloys in a low temperature, high magnetic field environment,[30-36] it is reasonable to suspect that the excess deformation-induced martensitic transformation will play a role in the fracture behavior. Indeed it is known that transformation can enhance ductility and fracture toughness of an alloy if it can be made to occur during deformation.[44-47] However, the details of fracture behavior in this type of environment have not been closely examined. Hence, the present work was undertaken to determine the extent and nature of the fracture toughness change of 304 stainless steel at 4.2 K in an 8 T magnetic field, and to determine and characterize the microstructural changes and associated mechanisms affecting the fracture toughness.

2. EXPERIMENTAL

Martensitic transformation is known to play a strong role in observed tensile behavior changes.[4,30-36] Therefore any changes that can be observed in the fracture

toughness in a magnetic field are also expected to be related to the in situ transformation. Thus austenitic stainless alloys of varying stabilities is examined to determine the effect of varying the amount of in situ transformation on the fracture behavior. The amount of transformation that can occur during the J_{IC} test is varied both through changes in chemistry and through prior deformation and transformation. Matched sets of specimens were tested at 4.2 K with 0 T and 8 T applied fields.

Chemistry-related stability changes were accomplished by using three types of austenitic stainless steel alloys, 304, 304L, and 310S. Stability increases in the order 304L, 304, and 310S.[4] AISI 304L is a low carbon variant of 304 and 310S is a high-Cr, high-Ni austenitic alloy. Both 304 and 304L undergo martensitic transformation with deformation at cryogenic temperatures while 310S is stable with respect to deformation-induced transformation to 4.2 K. The compositions of the 304, 304L, and 310S plates used in this work are listed in Table 1.

The amount of transformation available during crack initiation and propagation was controlled independently of chemistry by using 304L specimens with different prior deformation. Heavy prior deformation reduces the amount of in situ transformation by both causing a prior transformation and by stabilizing the austenite.[3,4,9,13] 304L plates were given a 20% reduction (31.8mm to 25.4mm) at 300 K and at 993 K. The 993 K treatment is well above the reversion temperature for 304L, so the plate should remain austenitic. Deformation at that temperature will, however, stabilize the alloy against subsequent transformation.[3] In addition, 304L plates were given a 13% (31.8mm to 27.6mm) rolling reduction at 77 K. Small amounts of plastic deformation at low temperature tend to increase planar defect density in low stacking fault energy alloys such as 304L and reduce the stability of the alloy.[4] Thus the order of the alloys in terms of increasing stability is 304L processed at 77 K, 304L, 304L processed at room

temperature, 304L processed at 993 K, 304 and 310S. Compact tension (CT) and tensile specimens were then machined from these plates. The specimen configurations are indicated in Figure 1.

J_{IC} tests were performed in an 8 T magnetic field at 4.2 K in the bore of a NbTi superconducting solenoid. The test facility is described in detail elsewhere.[30] A single specimen compliance technique, in which load line displacement measurements are made using a clip gage, was used. Crack growth was inferred from changes in specimen compliance during the test. The specimens were precracked at room temperature to a nominal a/w (ratio of the crack length to the distance between the knife edge and the back of the CT specimen) of 0.6. J_{IC} tests were conducted according to ASTM 813-88.

The 304L specimens that were cold-worked at 77 K contain significant amounts of martensite and were thus subject to brittle fracture. Thus valid J_{IC} measurements were not obtainable. Instead, matched sets of specimens with this processing were made into CT specimens suitable for use in K_{IC} tests in both 0 T and 8 T magnetic fields at 4.2 K. The specimens were precracked at room temperature to an a/w of 0.5. The tests were conducted according to ASTM399-83.

2.1 CALIBRATION

The strain gages used in the load cell and displacement gage have ferromagnetic components that can affect their output in a strong magnetic field. Since it is possible that the presence of the high-strength magnetic field can alter the response of the load cell and clip gage used in these tests, care was taken to calibrate the response of these instruments in the actual test conditions before each set of tests. The clip gage response was measured for a known imposed physical displacement (with a micrometer modified to work within the bore of the magnet) in the 8 T magnetic field at 4.2 K. The clip gage was placed at

approximately the position it would be during the actual tests and displacement imposed on the clip gage using the modified micrometer. Figure 2 shows the typical calibration change that occurs on application of the magnetic field at 4.2 K. The gage response is linear in both cases but a change in slope occurs on application of the 8 T field.

The LVDT (linear variable differential transformer) output was compared with actual displacements as determined with a micrometer both with and without the 8 T field and with the crosshead in its normal operating position. The load cell response at room temperature in the presence of the magnetic field was measured by placing the tensile load frame under constant stroke control and moving the crosshead, and thus the load cell, from approximately 2.5 m above the top of the solenoid bore to its normal operating position of approximately 1 m above the top of the bore. Any magnetic field influence on the output of the load cell would then be observable as a change in the output of the load cell on traversing the magnetic field gradient. The effects of the magnetic field on the load cell and the stroke LVDT displacement transducer were negligible.

2.2 MECHANICAL TEST PROCEDURE

In performing the J_{IC} tests with no imposed magnetic field at 4.2 K, the specimen was placed in constant load control and precooled to 77 K. It was then transferred to the cryostat, immersed in liquid He and cold-soaked for 5-10 minutes to allow the specimen to reach thermal equilibrium. The tensile machine was then placed in stroke control for the test. The same procedure was followed for tests in 8 T at 4.2 K. The crosshead was slowly lowered into position in the 8 T field and the liquid He and the specimen allowed to reach thermal equilibrium before the initiation of the loading and unloading cycles.

2.3 CHARACTERIZATION

Metallographic specimens were electroetched in a saturated aqueous solution of NaOH at 6 V to reveal grain boundaries and martensite transformation products. A 30-second etch in a solution of 20ml HCl, 100ml H_2O, and 1gm $K_2S_2O_5$ was used as an alternate treatment to reveal martensite and grain boundaries. The specimens were also coated with ferrofluid, a colloidal suspension of fine magnetic particles, to decorate the ferromagnetic martensite phase. Permeability and metallographic measurements were used to determine qualitatively and quantitatively the extent of the martensitic transformation. Crack profiles were made at the mid-plane of the CT specimens. The specimens were sectioned with an abrasive disk, and subsequently polished and etched, with care taken to preserve the edge adjacent to the fracture surface. The α' distribution within the transformation zone was determined by areal fraction measurements on 400X optical micrographs from the crack profiles. X-ray diffraction was performed on polished and slightly etched fracture profiles to detect preferred orientation in the transformed material.

Fractography was performed with SEM to obtain qualitative information on the fracture mode and small scale deformation features. There is a possibility that the difference in roughness created by differences in the martensitic transformation and subsequent deformation of the austenite matrix in the magnetic field could play a role in differences seen in the fracture toughness results. A more quantitative description of the fracture surfaces would serve to increase confidence in any conclusions drawn from qualitative interpretation of the fractographs. To quantify any differences in roughness and to provide a more sensitive measure, mechanical profilometry was performed on the fracture surfaces of the specimens on a 2mm x 4mm area near the fatigue precrack tip at the centerplane of the CT specimens. The profilometer used for this measurement has a

stylus tip with a 2.5 μm radius. Therefore the in-plane resolution of the instrument is on the order of 5 μm although it has a somewhat better detectability limit.

3. RESULTS

3.1 MECHANICAL TEST RESULTS

3.1.1 Tensile

The 4.2 K tensile data for the different alloys and processing conditions examined are listed in Table 2. With the exception of the 304L plates cold-rolled at 77 K, the macroscopic fractures modes were all ductile. The 77 K cold-rolled plates failed in a brittle mode after only 8% total elongation.

3.1.2 Fracture Toughness

The fracture toughness of the various alloys and processing conditions tested are presented in Figure 3. The values are $K_{IC}(J)$ except for the 77 K-rolled 304L. The 0 T and 8 T 77 K-rolled 304L conditions are from a valid K_{IC} measurement. The changes in fracture toughness between the various processing conditions for 304L are consistent with the changes in yield strength.

3.1.2.1 AISI 304

Both the T-L and L-T orientations of this alloy tested at 4.2 K in the 8 T field show $K_{IC}(J)$ values higher than those of the matching specimen tested without an applied magnetic field. In the T-L orientation, the average $K_{IC}(J)$ is 129 MPa-m$^{1/2}$ without an applied field and 179 MPa-m$^{1/2}$ with an 8 T field. In the L-T orientation, the average $K_{IC}(J)$ is 117 MPa-m$^{1/2}$ without an applied field and 151 MPa-m$^{1/2}$ with an 8 T field. The T-L fracture toughness is 38% higher and the L-T fracture toughness is 29% higher. The yield strength of the 304 plate at 4.2 K is 630 MPa in the longitudinal direction and 600 MPa in the long transverse direction (Table 2). The spread in the fracture toughness data

for each condition is extremely small, with almost no scatter in the 8 T, T-L orientation specimens. This is probably fortuitous rather than an indication of the accuracy or reproducibility of the tests since from experience a spread of 5-10% in the results can be expected from nominally identical specimens.

3.1.2.2 AISI 304L

The fracture toughness of 304L decreased slightly (~8%) with the application of the 8 T field at 4.2 K. The average $K_{IC}(J)$ value for the tests conducted with an applied field is 160 MPa-m$^{1/2}$, while the average value of those without an applied field is 175 MPa-m$^{1/2}$. This alloy was tested only in the L-T orientation.

3.1.2.3 Room Temperature-Rolled AISI 304L

The fracture toughness of 304L that had been subjected to 20% rolling reduction at room temperature also showed a negligible change with an 8 T applied field. The data show a ~4% improvement, which is within the limits of reproducibility of the test. The $K_{IC}(J)$ value without an applied magnetic field is 131 MPa-m$^{1/2}$ and 136 MPa-m$^{1/2}$ with an 8 T field.

3.1.2.4 Warm-Rolled AISI 304L

The fracture toughness of 304L that had been warm-rolled 20% at 993 K, showed a ~12% improvement in fracture toughness on application of an 8 T field at 4.2 K. The change is larger than the expected limits of reproducibility and thus should be reliable. The $K_{IC}(J)$ without an applied magnetic field is 149 MPa-m$^{1/2}$ and 166 MPa-m$^{1/2}$ with an 8 T field.

3.1.2.5 Cold-Rolled AISI 304L

The fracture toughness of 304L cold-rolled 13% at 77 K is extremely low at 4.2 K. This is anticipated since deformation at 77 K will cause strain-induced martensitic

transformation and subsequent testing at 4.2 K will be on a material with a high fraction of brittle martensite. The brittle failure mode for tensile tests conducted at 4.2 K confirms this suspicion. Since the failure mode will primarily be brittle, K_{IC} tests were performed on material with this processing rather than J_{IC} used for the more ductile materials. Only one valid test was obtained in each magnetic field condition due to difficulties in manufacturing the specimens. The K_{IC} value at 4.2 K is 66 MPa-m$^{1/2}$ without an applied field, less than half that of 304L without the 77 K processing. On application of the field, there was apparently further transformation during deformation that resulted in an atypical load-displacement record (Figure 4). The measured K_{IC} of this sample is 31 MPa-m$^{1/2}$ and it satisfied all other ASTM 399-83 requirements except that the load-displacement curve has a peculiar form. The shape of the load-displacement curve for the K_{IC} test in the 8 T magnetic field is similar to tensile stress-strain curves for metastable austenitic alloys, with a positive curvature after a small amount of displacement that is then followed by a negative curvature after further loading. This suggests that transformation ahead of the crack is causing a load relaxation and that the displacement being measured after a small amount of loading is not completely due to crack growth but instead is partially caused by the transformation strain.

3.1.2.6 AISI 310S

The fracture toughness of the stable 310S alloy showed negligible change with applied 8 T field. The ~4% decrease measured is within the limits of reproducibility of the test for nominally identical specimens. The average $K_{IC}(J)$ at 4.2 K for 310S was 283 MPa-m$^{1/2}$ without an applied magnetic field and 272 MPa-m$^{1/2}$ with an 8 T field.

3.2 CHARACTERIZATION

3.2.1 α' Distribution

The amount and the distribution of strain-induced martensite formed during testing varies with the stability of the alloy and with the applied magnetic field as shown through permeability and metallographic measurements. In general, more extensive transformation occurs in the less stable specimens. Application of an 8 T field increases the martensite content at a given distance from the crack plane, but does not always appreciably increase the transformation zone width.

3.2.2 AISI 304

Permeability measurements show that high permeability α' phase forms near the fracture surface. The amount decreases with distance from the fracture surface. Metallographic examination of fracture surface profiles confirm this observation (Figure 5). Beyond the observed plastic zone, α' was not found. The amount and extent of α' formation was qualitatively larger for the specimens tested in 8 T than for those tested in 0 T. In both cases, the martensite formed had the fine lath morphology seen previously in 18-8 stainless alloys[3-5].

The relative distributions of α' in the transformation zone as determined by metallographic measurements, are indicated in Figures 6 and 7. In both cases, the measured volume fraction of α' at a given distance from the crack plane was higher in the samples tested in the 8 T field than in the samples tested in zero field. The plate had a relatively large amount of sulfide particles aligned in the rolling direction. The difference in the fracture toughness values measured between the two orientations is primarily due to the presence of these particles.

X-ray diffraction on the fracture surfaces shows a slight difference in the 211 α' peaks between the 8 T and the 0 T specimens (Figure 8). However, the difference is so small that any texture difference in the α' induced by the magnetic field cannot be significant.

Fractographic examination shows a mixed mode fracture surface that is typical for 304 broken at 4 K; the fracture mode is primarily ductile with some secondary cracking and some relatively planar quasi-cleavage areas associated with α' (Figure 9). These planar features are similar to those reported by Reed et al.[27] and by Tobler and Meyn[29], who identified them to be (111) planes of the γ phase. The fracture surfaces of the specimens tested in 8 T and those tested in 0 T are qualitatively similar and have similar areal fractions of planar patches associated with α'. These planar areas are not true cleavage facets since they show some ductility. All specimens show some secondary cracking parallel to the plane of the CT specimens and perpendicular to the primary crack plane (Figure 10). Some splitting was also observed on the quasi-cleavage areas with the secondary crack planes parallel to the specimen face and perpendicular to the primary crack plane (Figure 11). These cracks are parallel to α'-γ laminate planes that are approximately perpendicular to the primary crack plane. The ductile-dimple areas of the 304 samples tested in the 8 T field were generally slightly less flat than those of the specimens tested without an applied field and appear to be more ductile (Figure 12).

Although the fracture surfaces appear qualitatively similar, analysis of the fracture surface profilometry data for the two magnetic field conditions reveal subtle differences. Typical real-space fracture surface profile traces for the two magnetic field conditions are shown in Figure 13a,b. Using the root mean squared (RMS) elevation as a convenient indicator of gross or long wavelength surface roughness, the two specimens are almost comparable (Table 3), 35 μm for the 8 T specimen and 30 μm for no magnetic field. The

normalized line lengths (Table 4) of the fracture profile traces, which indicate the amount of crack deflection from the propagation plane during fracture, are also slightly larger for the 8 T specimen: 1.11 compared to 1.07 for the 0 T specimen. The difference in the percentage of out of plane crack path lengths is not significant. However, when the data is converted into a frequency-space representation using a fast Fourier transform (FFT) and plotted as a difference of the normalized power spectrum of the 0 T and 8 T surface profiles (Figure 13c), an interesting difference emerges. The normalized power spectrum gives an indication of the proportion of the shorter wavelength, smaller components on the fracture surface relative to that of the longer wavelength features. The higher frequency components, which correspond to shorter wavelength features on the fracture surfaces, have similar relative values while the relative proportion of intermediate wavelength components are higher on the 8 T specimen fracture surface. Features with size greater than approximately 25 μm are proportionately greater on the 8 T specimen fracture surfaces.

3.2.3 AISI 304L

Permeability measurements near and on the fracture surfaces of CT specimens tested in both magnetic field conditions indicated some deformation induced transformation. This observation was confirmed with metallography on the polished and etched fracture profiles (Figure 14). The transformation zone width of the 304L L-T specimen for both 0 T and 8 T is larger than those of the 304 specimens tested, but does not show an appreciable difference in the transformation zone size as had the 304 specimens. The region of the specimen that had not undergone plastic deformation remained completely austenitic as determined from permeability and optical measurements.

Fractographic examination indicates a mixed-mode fracture, primarily ductile with some planar quasi-cleavage regions as in the 304 specimens. The appearance of the

fracture surfaces for both magnetic field conditions are qualitatively similar (Figure 15). Secondary cracks are also present on the fracture surfaces of specimens tested under both conditions. On a finer scale, the ductile-dimple areas of the specimens tested in the magnetic field appear generally flatter and coarser than those of the specimens tested without the magnetic field (Figure 16).

Profilometry data shows that the specimen tested in the 8 T magnetic field is rougher than the specimens tested without an applied field (Figure 17a,b). In contrast to the 304 specimens there is a substantial difference, the RMS elevation for the specimen profile shown is 36 μm for the 8 T case and 14 μm for the 0 T case. However, the normalized line lengths show the same amount of variation as for the 304LT specimens, 1.12 in the magnetic field as compared to 1.07 without an applied field. The difference spectrum (Figure 17c) also show that on the 0 T specimen fracture surface, features with intermediate and short wavelengths are proportionately more abundant relative to the coarsest features.

3.2.4 Room Temperature-Worked 304L

The 304L plates that were room temperature-rolled to a 20% reduction were partially transformed into martensite (Figure 18). The martensite volume fraction for the as-rolled plates is ~22%. The room temperature deformation-induced martensite can be distinguished from the 4.2 K deformation-induced martensite by its coarser and more wavy appearance. This difference is caused by the difference in slip characteristics of the parent austenite, along whose slip planes the martensite particles form, between rolling at room temperature and 4.2 K. The α' distribution as determined metallographically is presented in Figure 19.

Fractography indicates a mixed fracture mode, transgranular with some ductile regions for both magnetic field conditions (Figure 20). Secondary cracking perpendicular to the primary crack plane was also evident in both magnetic field conditions. The dimple areas of the specimens tested in the magnetic field appears slightly coarser and less flat than those of the specimens tested without a magnetic field (Figure 21).

Profile traces (Figure 22a,b) show that the 0 T specimen surfaces are slightly rougher than those of the 8 T specimen surface. The RMS elevation for the 0 T surfaces is 68 μm and is 46 μm for the 8T surfaces. The normalized line lengths are the same, 1.13, for both magnetic field conditions. The difference spectrum (Figure 22c) indicate that the 0 T surfaces have a higher fraction of short wavelength components than the 8 T surfaces while the opposite is true of the longer wavelength components.

3.2.5 Warm-Rolled AISI 304L

A 20% reduction of the 304L plate by rolling at 993 K serves to stabilize the austenite, reducing the amount of transformation which can occur during the subsequent 4.2 K deformation. The as-rolled plate is austenitic since rolling occurs above the M_d temperature for this alloy. The extent of the transformation zone for these specimens is similar for both magnetic field conditions (Figure 23).

Fractography indicates that the fracture surfaces are not qualitatively different (Figure 24); both magnetic field conditions show mixed-mode ductile and quasi-cleavage areas. Secondary cracking perpendicular to the primary crack plane is also observed for both magnetic field conditions. The dimple areas of the specimens tested in a magnetic field appears more ductile than those of the specimens tested without an applied field. Those tested without the magnetic field have a flatter appearance (Figure 25).

Surface profiles (Figure 26a,b) are fairly similar for the two magnetic field conditions. There is little difference in the RMS elevation for the two surfaces, 45 μm for the 8 T case and 39 μm for the 0 T case. The normalized line lengths are similar for both magnetic field conditions, 1.12 for the 8 T case and 1.10 for the 0 T case. The difference spectrum (Figure 26c) indicate that the 8 T fracture surfaces have a higher ratio of the short wavelength and long wavelength features with the 0 T surfaces having a higher ratio of features with components in the 95 μm to 140 μm range.

3.2.6 Cold-rolled AISI 304L

A 13% reduction at 77 K serves to transform the originally austenitic material to one that is partly martensite. The volume fraction was determined by x-ray diffraction measurements to be ~35% martensite.

The fracture mode of these specimens in both magnetic field conditions is mixed, with a relatively large fraction of quasi-cleavage areas interspersed in a ductile-dimple background. The 0 T surfaces have a higher fraction of transgranular areas than those of the 8 T surfaces (Figure 27). The dimple areas of the specimen tested in the magnetic field have a coarser, more angular appearance than those of the specimens tested without a magnetic field (Figure 28).

The real-space profiles of the fracture surfaces (Figure 29a,b) are fairly similar, with an RMS elevation of 44 μm for the 0 T case and 53 μm for the 8 T case. The normalized line lengths, 1.13, are the same for both magnetic field conditions. The difference spectrum (Figure 29c) indicate that the proportion of shorter and intermediate wavelength features to long wavelength features on the 0 T fracture surfaces is greater than that in the 8 T fracture surfaces.

3.2.7 AISI 310S

AISI 310S is a fully stable austenitic stainless steel under the test conditions used in this work. Permeability measurements on the fracture surfaces indicated that no detectable martensitic transformation had taken place during deformation at 4.2 K either with or without an applied magnetic field.

Fractography on these specimens shows that the fracture mode is ductile (Figure 30). There are no observable qualitative differences among the specimens tested with and without a magnetic field.

The profilometry data is shown in figure 31a,b. The real-space profiles are similar, with RMS elevation for the 8 T specimen being 61 μm and that for the 0 T specimen being 40 μm. The normalized line lengths, 1.12, are the same in both applied magnetic field conditions. The difference spectrum (Figure 31c) for the two test conditions show only very small differences in the proportion of short and intermediate wavelength to long wavelength features.

4. DISCUSSION

304 stainless steels are metastable, tending to transform from an fcc structure to a more stable bcc martensite at low temperatures. The transformation is driven by the free energy difference between the γ and the α' phases and is opposed by the increase in strain and surface energy due to the transformation. Increasing the free energy difference between the two phases at a constant temperature increases the driving force for the transformation at that temperature. Low temperature, mechanical stress, and the presence of a magnetic field will increase this free energy difference. Small amounts of prior plastic deformation below the M_d temperature also may facilitate transformation by promoting the nucleation of the martensite phase.[4,9] Thus the presence of these conditions will tend to

shift the transformation temperature upward and enhance the extent of the transformation to α'.

The effect of pulsed[29,17-22,24] and steady[23,28] magnetic fields on the martensitic transformation behavior of steels of various compositions has previously been examined. Those studies indicated that the amount of transformation was enhanced in the presence of a magnetic field. The extent of transformation was shown to be a function of field strength and independent of frequency and the number of applied pulses.[20] The presence of an applied field during transformation was also found to have an influence on the orientation distribution of the martensite that was formed.[51,52] The change in orientation distribution was attributed to the development of shape anisotropy of the martensite particles formed in the magnetic field with the easy magnitization axis aligned with the applied magnetic field.[52] The amount of magnetically induced α' is proportional to the product of the field strength and saturation magnetization difference between the parent γ and the product α' phase.[53]

During crack initiation and propagation, there is local deformation ahead of the crack tip due to the presence of a stress concentration. Therefore, a region exists ahead of the crack tip which has a higher transformation temperature than the bulk of the specimen and has a greater tendency to transform into α'. This tendency will be further increased by the presence of a magnetic field. This excess transformation product, above that expected from strain-induced transformation alone, and the timing of this transformation, i.e., whether the transformation is complete at an early stage of local plastic deformation or whether the transformation continues into the later stages of local plastic deformation, are expected to have an effect on fracture behavior.

Some probable effects of the transformation on the fracture toughness include: strain hardening rate increase due to the formation of α'; crack "shielding" due to dilatational and deviatoric components of the transformation strain acting to reduce the effective applied stress intensity on the crack tip; crack deflection and secondary cracking due to the presence of the harder α' phase in the γ matrix; and magnetostatic forces acting to reduce crack tip stress intensity. These mechanisms are all expected to be operating in parallel to some degree, increasing the measured fracture toughness. Possible mechanisms which act to reduce fracture toughness when α' forms ahead of the crack tip include increasing the effective stress intensity at the crack tip due to the transformation strain in the wedge-shape volume directly ahead of the crack tip bounded by angles of $\pm\pi/3$ from the crack plane[54,56-57] and providing bcc α'-containing regions of lower resistance to crack initiation and propagation at cryogenic temperatures.

4.1 Magnetostatic Effects

Magnetostatic forces can have an effect on the measurements done in this work. The volume of ferromagnetic α' formed during deformation in a magnetic field has a direct effect on the crack tip stress intensity and results in an extrinsic toughening mechanism. Modelled simplistically, the effect of the magnetic field on the stresses occurring at the crack during its opening and advance is analogous to the separation of plates of ferromagnetic material in a magnetic field. Since magnetostatic energy is minimized by containing the magnetic flux within the ferromagnetic material, the plates would tend to resist separation, with forces that can be calculated. Thus, during J_{Ic} tests on CT specimens in a solenoidal field, with the loading direction parallel to the solenoid axis, the formation of martensite around the crack would create a closing load on the crack. Since these tests were conducted under displacement control, there would be a higher recorded load per unit crack opening and advance in the magnetic field. The additional load is not present in tests conducted without a magnetic field, thus the measured applied energy per

unit crack advance is lower and the calculated J_{IC} and $K_{IC}(J)$ is lower than for in-field tests. This effect also should increase with crack extension to a certain extent since the martensite containing volume also increases, but should saturate rapidly since the rate of change in the volume occupied by the magnetic field in the low permeability region decreases rapidly with crack opening.

The magnitude of the magnetostatic interaction effect on measured J_{IC} can be estimated by considering the effect of the closing force on the crack tip stress intensity. Assuming the martensite saturation magnetization is the same as that of iron, there is 100% martensite near the crack surface, a straight crack front that has advanced 0.3 mm into martensite but has not separated, and no change in Young's modulus with applied field, an estimate of the upper limit to the change in measured fracture toughness due to magnetostatic effects is possible. The closing stress can be estimated by $0.5B^2/\mu_o$ where B is the induction field strength and μ_o is the permeability of vacuum. The stress intensity at the crack tip due to the closing force can be calculated using:[55]

$$K = -\sqrt{\frac{2}{\pi}} \int_0^d \frac{g(t)}{t^{1/2}} dt \qquad (1)$$

where t is the distance from the crack tip to a point behind the crack tip, d is the span over which the closing stresses act, and g(t) is the closing stress on the crack.

The results of this calculation indicate a negative contribution to the crack stress intensity on the order of 1 MPa-m$^{1/2}$. This represents only approximately 3% of the fracture toughness improvement in the T-L and approximately 2% in the L-T 304 specimens and a proportionately larger percentage of the fracture toughness of the other specimens since they show a smaller fracture toughness change with applied magnetic field. This suggests that although the magnetostatic interaction does contribute to the fracture toughness improvement, the magnitude of the contribution is relatively small and

will be masked by the scatter in the fracture toughness data in materials with relatively high toughness.

4.2 Crack Tip Shielding Effects

Another fracture toughness enhancing mechanism that can be associated with increased martensite formation is the increased shielding effect of the excess volume of martensite. It is known that martensitic transformation, when properly situated both spatially and temporally with respect to the crack, can toughen a material.[54,56] The volumetric expansion associated with the formation of martensite alters the stress intensity at the crack tip. 304 is thermally and magnetically stable unless plastic deformation at cryogenic temperatures occurs; then the martensite forms within the plastic zone of the crack. This zone is bounded by material which remains elastic and thus has not transformed. The volume expansion due to martensite formation is therefore constrained by the elastic untransformed material, altering the stress field around the crack. If the martensite is behind a front bounded by angles of $\pm\pi/3$ with respect to the crack plane, the dilatation will impose a compressive stress, decreasing the effective stress intensity at the crack tip. The measured fracture toughness would thus increase. If transformation occurs in the wedge ahead of the crack tip bounded by the front, the dilatation results in a tensile stress on the crack tip, thus increasing effective stress intensity and decreasing measured fracture toughness.

The magnitude of the change in stress intensity, ΔK, can be calculated. This stress intensity change is a function of the transformation strain, transformation zone size and geometry, and volume fraction transformed. Under plane strain conditions, the contribution to ΔK due to dilatation of a volume of transformed material is given by:[54,56]

$$\Delta K = \frac{E}{3\sqrt{2\pi}\,(1-\upsilon)} \int_A \theta\, r^{-3/2} \cos\frac{3}{2}\phi \, dA \qquad (2)$$

where ΔK is K_{tip}-K_∞, the stress intensity difference induced by the transformation, E is Young's modulus, υ is Poisson's ratio, θ is the in-plane strain due to transformation in an element dA (i.e. product of the local volume fraction transformed and the transformation strain), r is the distance from the crack tip, ϕ is the angle from the primary crack plane to dA, and A is the area of the transformation zone on one side of the crack plane.

The magnitude of this toughening mechanism in the alloy that shows the greatest change in fracture toughness with magnetic field can be estimated by using the observed zone shape and α' distributions. Numerically integrating equation 2 using the transformation zone shape illustrated in Figure 32 and α' distributions (Figure 6,7) observed for the 304 specimens, under the assumption that the zone shape remains geometrically similar during crack initiation and growth (i.e., the zone front geometry and zone height remain constant during crack growth with only the length of the zone changing as the crack grows) and that the relationship, $K^2 = JE$, is valid in this case, will provide an estimate of the magnitude of the fracture toughness increase due to this mechanism. The α' fraction is assumed only to vary with y, the distance from the crack interface. The observed α' area fraction profile for 304 (Figure 6) is fitted to an equation of the form $f(y)=A10^{By}$ (where A and B are fitting parameters, y is the distance along a normal to the crack plane, and f(y) is the α' areal fraction in the neighborhood of y). f(y) is then multiplied by the dilational transformation strain to obtain a local θ in equation 2. The integration is performed for a sequence of increasing crack lengths to obtain the ΔK behavior with crack growth. If the stress intensity difference increases rapidly enough

with crack extension, it will be reflected in the measured J values. The results for the L-T case (Figure 33) show that the difference in stress intensity approaches its limiting value at a crack extension of 0.3 mm, close to the start of valid data points as specified by ASTM 813-87, and thus should cause a detectable difference in the measured fracture toughness. A decrease in the stress intensity at the crack tip between the applied field and zero field cases of approximately 2.3 MPa-m$^{1/2}$ is predicted. This is an order of magnitude less than the observed difference of approximately 35 MPa-m$^{1/2}$ in fracture toughness for the 304 LT specimen. However, this mechanism will constitute a larger fraction of the observed difference for the RT-rolled material since the extent of the transformation zone is larger. But the increase in toughening varies as the square root of the transformation zone width.[54] Therefore the contribution of this mechanism to the fracture toughness increase of RT-rolled 304L is on the order of twice that calculated for 304. In the 993 K-rolled 304L plate and the as received 304L plate, both the martensite profile and the transformation zone width are substantially the same, thus this mechanism cannot contribute significantly to the observed fracture toughness changes.

This calculation, however, assumes isotropic dilatational effects only. Some attempts at modelling the transformation shear strain and transformed particle shape on the stress intensity at the crack tip indicate that the calculated stress intensity difference can be greater[57]. If the shear strain is included, and is assumed to be completely relaxed in such a way as to cause uniaxial dilatation in the direction of maximum principal strain, and the transformation occurs only at the transformation zone front, the stress intensity difference will increase substantially. Calculations with this assumption using a zone contour which assumes transformation at maximum principal stress[57] yield a ΔK approximately 2.5 times larger than that obtained by just assuming isotropic dilatation on transformation. However, it is unlikely that the transformation shear strains will have a large effect on the fracture toughness in the alloys tested since the macroscopic shear strains, which are of

importance here, will be small to negligible. The martensite particles in these alloys have been observed to form in a self-accomodating manner that minimizes macroscopic shear strains.[3,4]

There is a further decrease in the crack tip stress intensity for certain orientations of the transformed particles with respect to the crack if the transformed particle shape is non-spherical.[57] Under the assumption that the particles are high aspect ratio ellipsoids with the major axis oriented parallel to the primary crack plane, it was shown that an increase in $\Delta K_{tip}/K_{tip}$ over that of the pure isotropic dilatational case is possible. With the Young's modulus and the typical transformation zone size for the 304 specimens, up to a six-fold decrease in $\Delta K_{tip}/K_{tip}$, depending on the martensite particle aspect ratio, is predicted. This will bring the predicted fracture toughness change due to excess martensite formation closer to the measured fracture toughness change, assuming the model is accurate. An upper limit of about 10 to 12 MPa-m$^{1/2}$ due to the shielding effect of the excess martensite in the magnetic field is possible, but it is still several times less than the measured difference in the AISI 304 specimens. Although there is evidence of shape anisotropy in the bcc phase formed Fe-V and Fe-Ni alloys in 0.6T fields,[52] the magnitude of anisotropy detected is much smaller than that assumed in the theoretical model described above. The general crystallographic orientation-particle shape relationship is fixed for 18-8 type alloys,[3-5] therefore shape anisotropy will be seen in crystallographic texture data. X-ray diffraction measurements on the fracture surfaces of the 304 specimens do indicate a slight difference (Figure 8), but the differences between the two magnetic field conditions are very slight, indicating a small anisotropy difference between the samples. Therefore, any anisotropy caused by the α' formation in the magnetic field will not contribute significantly to the measured difference in fracture toughness. Thus the crack tip stress intensity reduction due to the dilatational transformation strains and transformed particle

shape anisotropy can account for only a small part of the observed fracture toughness increase.

4.3 Strain Hardening Rate Effects

Comparison of the tensile deformation behavior of 304L and 304LN stainless steels with a high strength magnetic fields and without an applied magnetic field at 4.2K indicates that there is no detectable change in the yield strength between the two cases, but there are differences in the post yield deformation behavior due to transformation to α'.[34] In a magnetic field, the specimens show a slight reduction in flow stress right after yield and a higher strain hardening rate at higher strains than specimens tested without a magnetic field. This behavior was attributed to the excess transformation induced by the magnetic field. A portion of the externally imposed elongation is accommodated by the transformation, reducing the load required for a given imposed strain. At the higher strains the deformation is taken up by the retained austenite in which slip occurs through a progressively denser distribution of hard α' particles, their associated strain fields and the dislocations produced during the transformation. This behavior occurs both in the 304L and 304LN alloys with greater effects seen in the less stable 304L. The effect also increases with decreasing temperature. 304L and 304LN bracket 304 in terms of stability with respect to transformation to α'. Thus 304 should respond in the same manner and should show an increase in strain hardening rate in the uniform elongation regime when deformed at cryogenic temperatures in a strong magnetic field. This difference in strain hardening rate behavior is expected to result in more diffuse deformation (i.e. relaxation of the HRR strain singularity) in the CT specimens, distributing damage over a larger volume of the material tested in a magnetic field than for that tested without an applied field. Fultz and Morris[34] found that over most of the range of uniform elongation both 304L and 304LN had higher strain hardening rates when tested in an applied field. This difference increased with increasing true strain. The total elongation can either increase or decrease

with magnetic field depending on the amount of prior thermomechanical treatment; annealed material had a slightly greater elongation while worked material showed a slight decrease.[36] A material with a higher strain hardening rate, if all other factors were constant, would absorb more energy per unit imposed strain. The increase in strain hardening rate with applied field thus would allow the transformed volume of material to absorb more energy for a given imposed strain in the magnetic field. Fracture toughness has been modelled as a function of various material microstructural and tensile parameters,[58-62] and for ductile mode fractures, varies either implicitly or explicitly with the strain hardening rate of the material. Thus the increased strain hardening rate seen with the increased martensite transformation should contribute to increased measured fracture toughness. Fultz, et al.[34] show maximum strain hardening rate differences of 10% and 17% between the 0 T and the 18 T cases for 304LN and 304L respectively at 77 K. If the differences for 304 at 4.2 K are comparable, then we should expect a similar difference in the fracture toughness. Precise quantitative estimates, however, are difficult to make because of the geometry of the transformation zone and the nonuniform distribution of martensite and local strain hardening rate therein. It is also not clear that the existing models accurately reflect the conditions in this case since the material clearly does not remain homogeneous during fracture but transforms locally. It is the local strain hardening rate and failure strains that are important to the fracture process and that are changed by the local transformation. This is reflected qualitatively in the differences seen in the ductile areas of the fracture sufaces. Assuming that the trends predicted by these models still qualitatively hold for the specimens tested here, then the fracture toughness differences will scale with strain hardening rate differences and thus the magnitude of the fracture toughness differences is on the same order as the strain hardening rate differences. Therefore the increased strain hardening rate, assuming all else remain constant, should increase the fracture toughness of the least stable alloy, the as-received 304L, in the 8 T magnetic field. But this is not the case. On the contrary, the as-received

304L has a slightly lower fracture toughness in the 8 T field. Thus the strain hardening rate does not always dominate in producing the measured fracture toughness difference, at least not in the as-received 304L.

4.4 CRACK DEFLECTION

Crack deflection at hard second phase particles can potentially produce an increase in the effective fracture toughness by increasing the real crack propagation path lengths. In addition it can increase apparent mode I fracture toughness by allowing mode II cracking. The energy absorbed during the mode II cracking is then included in the determination of K_I. But it is unlikely that crack deflection is a major factor in the differences in fracture toughness between 0 T and 8 T.

Surface roughness can be used as an indication of the amount of crack deflection that has occurred. The RMS elevation from the mean line of the fracture profile (Table 3) and the normalized line lengths (ratio of actual line length to projected line length) of the surface traces (Table 4) can be used to indicate the relative degree of the coarse scale roughness and therefore the degree of crack deflection. From these indications, crack deflection appears to play a very minor role, if at all on the measured fracture toughness differences.

If the RMS elevation of the fracture surface from its mean plane is used as an indication, it would appear that only the RT-rolled 304L condition should show fracture toughness degradation at 8 T. However, the fracture toughness of only the as-received 304L and the 77 K-rolled 304L showed a decrease at 8 T, the others either had no significant change or improved with the application of the 8 T field. If the normalized line lengths are used as an indication of the amount of deflection, the conclusion is the same. There is no clear relation between amount of crack deflection and the direction of fracture

toughness change in an 8 T magnetic field. Both 304 LT and the as-received 304L had approximately the same difference between the two magnetic field conditions, with a slightly higher projected line length for the 8 T field in both cases. Thus if crack deflection were a major factor, there should be an increase in fracture toughness with applied magnetic field in both cases. What is observed is an improvement for the 304 LT case and a degradation in the as-received 304L case. The normalized line lengths are approximately the same for both magnetic field conditions in each of the other alloys and processing conditions, regardless of the magnitude of the observed fracture toughness changes. Therefore the crack deflection cannot be a major contributor to the changes in fracture toughness observed within the 8 T magnetic field at 4.2 K.

4.5 Fracture Micromode Effects

The fracture mode of the 304 CT specimens tested with and without an applied magnetic field is primarily ductile void coalescence interspersed with some α'-γ delamination in grains favorably oriented with respect to the primary crack plane. The amount of delamination seen in both cases (with and without an applied field) is qualitatively similar. This implies that the changes seen in fracture toughness between material tested in the 8 T field and material tested without an applied field are unlikely to be significantly affected by α'-γ delamination differences.

Secondary cracking can affect measured fracture toughness by absorbing some of the applied energy and reducing the stress triaxiality ahead of the crack tip. However, the amount of secondary cracking induced by the magnetic field and by the excess α' formed over that already present due to the plastic deformation is expected to be small. Secondary cracking is observed in all the specimens tested, but the difference in the amounts of secondary cracking between the applied field and zero field specimens are not readily apparent. Both conditions have qualitatively similar amounts of secondary cracking. If

there are effects on fracture toughness due to the formation of secondary cracks, they are not of great significance in these specimens.

Profilometry data on the 304 fracture surfaces (Figure 13), however, indicate a subtle difference in the fracture surface characteristics. The power spectrum of the fracture surfaces near the centerplane of the CT specimens which were tested in the magnetic field, just beyond the fatigue precrack, show a shift towards shorter wavelengths components. The difference spectrum (between the 0 T and 8 T specimens) formed from the normalized power spectrum shows that the 8 T case has higher levels of short and intermediate wavelength components relative to the longest component. This indicates that the fracture surface features of the specimens tested in the magnetic field are of a finer scale. Although it can be argued that a higher volume fraction of void nucleation sites, such as inclusions, will produce the same difference in the power spectrum by reducing the microvoid separation, it is not the case here. These specimens were machined from the same plate, and it is unlikely that the inclusion density or microstructure will vary significantly. Thus the difference spectrum implies a more homogeneous deformation in the 8 T specimens. This is consistent with the observation of Fultz et al.[30], in long gage length 304L and 304LN tensile specimens subjected to a constant strain at 77 K with half of the gage section exposed to a 16 T pulsed magnetic field, that a difference in deformation occurs because of the applied magnetic field. The half that was in the bore of the solenoid showed a finer more dispersed slip pattern than that of the half that was outside of the bore. This type of behavior is consistent with the larger fraction of finer fracture surface features of the specimens tested in the magnetic field and consistent with the higher strain hardening rates in the magnetic field. The fracture surfaces observed consist of some relatively planar areas in a matrix of ductile microvoid containing regions which failed through microvoid coalescence. Thus the fracture process consists of the linkup of quasi-cleavage areas through the microvoid regions and therefore the fracture

toughness is likely to be strongly influenced by the failure of the more ductile microvoid regions. A more homogeneous deformation behavior in the microvoid regions would increase the absorbed energy during fracture.

Similarly, the RT-rolled and the 993 K-rolled 304L specimens, which show improvements in fracture toughness in the magnetic field, show an increase in the proportion of intermediate and short wavelength features on the fracture surfaces of the 8 T specimens. This is consistent with improvements in fracture toughness because of a more homogeneous slip behavior. Conversely, the difference spectrum for the as-received 304L specimen tested without an applied magnetic field show a higher proportion of intermediate and short wavelength components on the fracture surfaces. The decrease in fracture toughness for this alloy condition in the magnetic field is thus consistent with a less homogeneous slip behavior. AISI 304L is the least stable of the alloys tested. Although it has a higher strain hardening rate in the magnetic field, its low stability augmented by the magnetic field may cause it to transform prematurely in the strain field ahead of the crack. Thus the crack would grow and advance into a low toughness region.

This can readily be seen by considering the stress and plastic strain distribution ahead of a crack tip. A schematic illustration of the tensile stresses and plastic strains ahead of a blunt notch[38] and a blunted crack in a power-law strain hardening material[64,65] is shown in Figure 34. The stress peaks in front of the crack and drops with distance, while the plastic strain is at a maximum at the crack and decays rapidly with distance. The peak is more pronounced and shifts toward the crack tip with higher strain hardening. The growth of the crack into a material can be considered from the coordinate system of the crack tip as the motion of volume elements of material toward the crack tip through its associated stress and strain fields. A volume element of lower stability with respect to

deformation-induced transfomation will initiate transformation at low plastic strains while a more stable volume element will commence transformation at higher plastic strains.

Consider the two extreme cases of transformation initiating at low plastic strain, point A, and at high plastic strain, point B, in Figure 34. For case A, as the crack grows, or equivalently as the volume element traverses the stress and strain fields toward the crack tip, the volume element is subjected to increasing plastic strains which drive the transformation toward completion. Assuming the shape of the stress and strain fields are substantially the same even with local transformation, this α' containing transformed volume element is then subjected to the progressively higher tensile stresses as it travels toward the crack tip from where it initially transformed. For case B, the more stable condition, the transformation is delayed to beyond the peak stress region where the plastic strains are higher. It would thus have initiated microvoid formation and coalescence prior to transformation to a low toughness volume. The transformed element is then subjected to progressively lower tensile stresses as the crack grows. If the criterion for fracture of the α' containing volume elements is the achievement of a critical stress over a critical distance[39], and if this criterion can be applied to quasi-cleavage cracks in these alloys, then case A should be more susceptable to quasi-cleavage fracture and should have lower fracture toughness than case B, assuming that the transformation does not relax the peak stress to below the critical fracture stress. Except for the AISI 310S, the alloys tested lie between these two extremes. Transformation occurs all along the strain path after initiation, with the extent of transformation dependent on the stability of the material. Thus the strength of this mechanism will vary with the material stability.

The amount of fracture toughness degradation for a transformed volume of the material is indicated by the measured toughness of 77 K-rolled 304L at 4.2 K. Although the processing only produced a 35% volume fraction of α', its K_{IC} is reduced to 66 MPa-

$m^{1/2}$. We should thus expect to observe a lower fraction of the ductile-dimple areas relative to quasi-cleavage areas on the fracture surfaces of the alloys tested in the magnetic field if the stability change caused by the magnetic field shifts the transformation initiation point to low plastic strains and a higher α' fraction is formed before the peak tensile stress region is reached. This would change the relative amounts of higher energy absorbing ductile-dimple regions to lower energy quasi-cleavage regions. This behavior is consistent with the differences observed in the fracture toughness and the fracture surfaces for the different alloys tested. The least stable alloys, the as-received 304L and the 77 K-rolled 304L, show a decrease in fracture toughness with an applied 8 T field while the others with higher stability show progressively higher toughness with stability in the magnetic field (Figure 35). This is consistent with the difference spectrum for the as-received 304L specimens which indicate a lower proportion of short to intermediate wavelength components for 8 T specimen as compared to 0 T specimen and with the difference spectrum for the RT and 993 K-rolled specimens which show higher proportions of the intermediate and short wavelength features.

The behavior is consistent with the later data of Fukushima et al.,[48] who tested AISI 304 in 0 T and 8 T magnetic fields with different precrack conditions. Precracking at 77 K introduced a transformed zone ahead of the crack containing the α' phase before the subsequent J_{IC} tests at 4.2 K. This reduced the measured J_{IC} as compared to specimens precracked at 300 K since the crack is initiating and growing into an α' containing region. Deformation at the different temperatures also can cause a difference in the stability[4,13] over part of the region ahead of the crack. The specimens precracked at 300 K showed higher fracture toughness at 8 T than at 0 T, consistent with the data presented here. The 77 K precracked specimens show a lower J_{IC} at 8 T. This behavior is consistent with the early α' formation ahead of the crack as has occurred in the as-received 304L specimens tested here. If the transformation which occurred during precracking has not reached a

point where the retained austenite is stabilized against further transformation, exposure to the 8 T field would tend to increase the amount of α' in the strain field ahead of the crack, producing a region of decreased toughness.

Thus in a magnetic field, the average amount of α' formed around the crack can increase and the observed α' profile near the crack plane is shifted to higher values. A number of mechanisms, all related to the appearance of the ferromagnetic α' phase, are operating in parallel to alter the stress intensity at the crack tip. The dominant effects are due to shielding and magnetostatic interaction. The stress field around the crack tip is altered due to the martensitic transformation, decreasing the effective stress intensity. A comparable reduction in effective stress intensity is produced by magnetostatic interaction. In addition, the higher strain hardening rate and the more homogeneous deformation in the magnetic field serves to diffuse damage, if local quasi-cleavage fracture does not become dominant, thereby contributing to an increase in measured fracture toughness of the specimens tested in an 8 T field.

Conversely, the early appearance of martensite ahead of the crack tip increases the propensity for quasi-cleavage and causes a reduction in fracture toughness. This tendency is enhanced by the presence of a magnetic field which encourages transformation. All of these mechanisms are in effect to some extent, with their importance to the fracture toughness a function of the stability of the alloy in the test environment. If the stability is such that significant early transformation occurs, then quasi-cleavage increases and becomes more dominant in its effect on the fracture toughness and its reduction in the magnetic field. If the stability is such that significant transformation is delayed to high plastic strains, on the decreasing side of the tensile stress peak ahead of the crack, then the other factors, increased strain hardening rate, homogeneous deformation, transformation toughening, and magnetic interaction become more dominant, increasing the fracture

toughness in the magnetic field. The proposed explanation for the fracture toughness differences in the magnetic field is not inconsistent with the slight decrease in the fatigue crack growth rates of 304L and 304LN in a magnetic field[30] at 77 K where the ΔK was limited to less than 60 MPa-m$^{1/2}$. The magnetostatic interaction contribution would not be reflected in the data in that case since their fatigue tests were performed under load control.

It is also consistent with data first reported by Fukushima et al.[37] They reported a decrease in J_{Ic} with application of a magnetic field and suggested that their results can be explained in terms of a theory developed by Shindo[40-42], which predicts an increase in crack tip stress intensity for a crack in a magnetically soft elastic body in a magnetic field oriented normal to the crack plane. However, the assumptions used in deriving the theory do not correspond to what is actually happening. The ferromagnetic phase in the test specimens develops in the presence of the magnetic field during deformation and is localized to an area around the crack. It is thus nonuniformly distributed rather than the uniform body assumed in the theory. It also does not consider the changes in material's deformation behavior in the magnetic field. Furthermore, the theory was developed for small field strengths and assumed a linear increase in magnetic susceptibility with field. However the disparity can be resolved if the difference is assumed to be due to differences in stability and specimen preparation procedures. The stability and thus the mechanical properties of 304 are sensitive to factors such as its C, N, and Ni content and grain size.[11,16,49,50] The 304 alloy used in this experiment may differ in stability from that used by Fukushima et al.[37] due to differences in these factors. Also their precracking was performed at 77 K which can further influence stability in the region ahead of the crack causing the quasi-cleavage micromode to become more dominant in a magnetic field, reducing fracture toughness. That this is happening is indicated by his later data which examines AISI 304 fracture toughness with different precrack conditions.[48] Precracking

at room temperature improves fracture toughness in a magnetic field while precracking at 77 K reduces toughness.

The engineering implication is that the fracture toughness of these metastable alloys is strongly environment sensitive with its sensitivity derived from its stability through its precise chemistry and processing. Therefore, testing which closely reproduces expected environments and failure modes during actual use should be considered for fracture toughness critical applications with these alloys.

5. CONCLUSIONS

The fracture toughness of metastable alloys in a cryogenic environment can be changed with the application of a high strength magnetic field. This variation is related to the timing of martensite formation during deformation and thus to alloy stability that, in turn, is dependent on its chemistry and processing history. A number of different processes appear to be operating in parallel to produce this variation in fracture toughness with magnetic field, with the relative importance of a particular process dependent on where the transformation occurs with respect to the crack tip.

Crack deflection does not play a significant role in the observed changes in fracture toughness.

Magnetostatic interaction serves to decrease crack tip stress intensity in a magnetic field, but its magnitude is small.

Transformation toughening also improve fracture toughness by decreasing crack tip stress intensity. The magnitude of this mechanism as estimated by current continuum

models, although larger than that of the magnetostatic interaction, is still relatively small and cannot adequately account for the differences observed in the fracture toughness.

Fracture micromode changes, the propensity for local quasi-cleavage due to the appearance of the brittle α' phase, is an important factor if early transformation occurs due to the destabilizing influence of the magnetic field.

Strain hardening and diffused deformation due to the formation of excess martensite in the magnetic field appear to be an important factor in the increased fracture toughness, if the fracture micromode changes do not dominate.

The engineering implication is that careful characterization must be done on these types of alloys if they are to be considered for use in fracture toughness critical applications in high magnetic field, cryogenic environments.

6. SUGGESTED FUTURE WORK

It is extremely difficult to separate and accurately quantify the contributions of the various mechanisms causing the change in fracture toughness with magnetic field since they are simultaneously active over a small region near the crack tip. But it would be of interest to more fully quantify the effects of local strain hardening and diffused deformation on the fracture toughness differences.

7. REFERENCES

1. Cook, D. C., Met. Trans. A, 18A, Feb. 1987, pp. 201-210.
2. Mangonon, Jr., P. L., Ph.D. Thesis, University of California, Aug. 1968.
3. Reed, R. P., Acta Metall., 10, Sept. 1962, pp.865-877.

4. Reed, R. P., Martensitic Phase Transformations, Materials at Low Temperatures, R. P. Reed and A. F. Clark, eds., American Society for Metals, Metals Park, Ohio, 1983, pp. 295-341.

5. Venables, J. A., Phil. Mag., 7, Jan. 1962, pp. 35-44.

6. Kelly, P. M., Metallurgical Developments in High-Alloy Steels, Proceedings of a Joint Conference on High-Alloy Steels, June 1964, pp.146-161.

7. Kelly, P. M., Acta Metall., 13, June 1965, pp. 635-646.

8. Kelly, P. M. and J. Nutting, Journal of the Iron and Steel Institute, 197, Mar. 1961, pp. 199-211.

9. Strife, J. R., M. J. Carr, and G. S. Ansell, Met. Trans. A, 8A, Sept. 1977, pp. 1471-1483.

10. Breedis, J. F. and W. D. Robertson, Acta Metall., 11, June 1963, pp. 547-569.

11. Breedis, J. F. and W. D. Robertson, Acta Metall., 10, Nov. 1962, pp.1077-1088.

12. Breedis, J. F., Trans. of the Metallurgical Society of AIME, 230, Dec. 1964, pp. 1583-1596.

13. Lagneborg, R., Acta Metall., 12, July 1964, pp. 823-843.

14. Suzuki, T., H. Kojima, K. Suzuki, T. Hashimoto, and M. Ichihara, Acta Metall., 25, 1977, pp. 1151-1162.

15. Suzuki, T., H. Kojima, K. Suzuki, T. Hashimoto, and M. Ichihara, Scripta Metall., 10, no. 4, April 1976, pp. 353-358.

16. Nishiyama, Z., Martensitic Transformation, Academic Press, New York, 1978, pp. 299-336.

17. Voronchikhin, L. D. and I. G. Fakidov, Fiz. Metal. Metalloved., 24, no. 3, 1967, pp.459-462.

18. Malinen, P. A., V. D. Sadovskiy, and I. P. Sorokin, Fiz. Metal. Metalloved., 24, no. 2, 1967, pp. 305-309.

19. Romashev, L. N., I. G. Fakidov, and L. D. Voronchikhin, Fiz. Metal. Metalloved., 25, no. 6, 1968, pp. 1128-1130.

20. Sadovskii, V. D., N. M. Rodigin, L. V. Smirnov, G. M. Filonchik, and I. G. Fakidov, Fiz. Metal. Metalloved., 12, no. 2, 1961, pp. 302-304.

21. Fokina, Y. A., L. V. Smirnov, and V. D. Sadovskiy, Fiz. Metal. Metalloved., 27, no. 4, 1969, pp. 756-757.

22. Malinen, P. A. and V. D. Sadovskiy, Fiz. Metal. Metalloved., 28, no. 6, 1969, pp. 1012-1017.

23. Fokina, Y. A., L. V. Smirnov, V. D. Sadovskiy, and A. F. Peikul, Fiz. Metal. Metalloved., 19, no. 6, 1965, pp. 932-933.

24. Fior, G. O., Ph.D. Thesis, University of California, Berkeley, 1984.

25. Malinen, P. A. and V. D. Sadovsky, Phys. Met. Metall., 1966, 21, no.5, pp. 139.

26. Peters, C. T., P. Bolton, and A. P. Miodownik, Acta Metall., 20, July 1972, pp. 881-886.

27. Reed, R. P., P. T. Purtscher, and K. A. Yushchenko, Adv. in Cry. Eng. Mat., 32, 1986, pp. 43-50.

28. Krivoglaz, M. A. and V. D. Sadovsky, Fiz. Metal. Metalloved, 1964, 18, no. 4, p. 502.

29. Tobler, R. L. and D. Meyn, NBSIR 85-3025, 1985, pp. 167-179.

30. Fultz, B., G. M. Chang, and J. W. Morris, Jr., Austenitic Steels at Low Temperatures, Plenum Publishing Corp, New York, 1983.

31. Bolshutkin, D. N., Desnenko, V. A., and Ilichev, V. Ya., Cryogenics, 19, 1979, pp. 231-234.

32. Goldfarb, R. B., R. P. Reed, J. W. Ekin, and J. M. Arvidson, Adv. Cry. Eng.-Mat., 30, 1984, pp. 475-482.

33. Reed, R. P., J. M. Arvidson, J. W. Ekin, R. H. Schoon, Austenitic Steels at Low Temperatures, Plenum Press, 1983, pp. 187-198.

34. Fultz, B. and J. W. Morris, Jr., Acta Metall., 34, no. 3, 1986, pp. 379-384.

35. Fultz, B., G. O. Fior, G. M. Chang, R. Kopa, and J. W. Morris, Jr., Adv. Cry. Eng. - Mat., 32, 1986, pp. 377-384.

36. Fultz, B., G. M.Chang, et. al., Adv. Cry. Eng. - Mat., 30, 1983, pp. 253-262.

37. Fukushima, E., S. Kobatake, M. Tanaka, and H. Ogiwara, Adv. Cry. Eng. - Mat., 34, 1988, pp. 367-370.

38. McMeeking, R. M., J. of Mech. and Phys. of Solids, 25, 1977, pp. 357-381.

39. Ritchie, R. O., J. F. Knott, and J. R. Rice, J. of Mech. and Phys. of Solids, 21, 1973, pp. 395-410.

40. Y. Shindo, Trans. of the ASME, 50, Mar. 1983, pp. 50-56.

41. Y. Shindo, J.of Appl. Mech., 44, Mar. 1977, pp. 47-51.

42. Y. Shindo, J. of Appl. Mech., 45, June 1978, pp. 291-296.

43. Yanagi, H., A. Nyilas, and W. Specking, KfK report no. 030306P15D, Aug. 1988.

44. Antolovich, S. D. and B. Singh, Met. Trans., 2, Aug. 1971, pp. 2135-2141.

45. Parker, E. R. and V. F. Zackay, Eng. Fract. Mech., 5, 1973, pp.147-165.

46. Birat, J. P. and W. W. Gerberich, Int. J. of Fract. Mech., 7, 1971, pp. 108-110.

47. Zackay, V. F., E. R. Parker, D. Fahr, and R. Busch, Feb 1967, Trans. ASM, 60, 1967, pp. 252-259.

48. Fukushima, E., S. Kobatake, M. Tanaka, and H. Ogiwara, presented at the 11th Conference on Magnet Technology, Tsukuba, Japan, Sept 1989.

49. Pickering, F. B., Int. Met. Rev., no. 211, December, 1976, pp. 227-268.

50. Tobler, R. L. and R. P. Reed, NBSIR 81-1645, pp. 101-129.

51. Ohashi, N. and S. Chikazumi, J. Phys. Soc. Japan, 21, 1966, p. 2086.

52. Yermolayev, A. S., A. Z. Menshikov, and P. A. Malinen, Fiz. Metal. Metalloved., 26, no. 1, 1968, pp. 76-80.

53. Satyanarayan, K. R. and A. P. Miodownik, Mechanism of Phase Transformation in Crystalline Solids, Institute of Metals, Monograph no. 33, pp. 162-166.

54. McMeeking, R. M. and A. G. Evans, J. Am. Cer. Soc., 65, no. 5, 1982, pp. 242-246.

55. Tada, H., The Stress Analysis of Cracks Handbook, Paris Productions, St. Louis, MO, 1985.

56. Budiansky, B., J. W. Hutchinson and J. C. Lambropoulos, Int. J. Solids Struct., 19, no. 4, 1983, pp. 337-355.

57. Lambropoulos, J. C., Int. J. Solids Struct., 22, no.10, 1986, pp. 1083-1106.

58. J. M. Krafft, Applied Materials Research, 1, 1964, pp. 88-101.

59. Ritchie, R. O., W. L. Server, and R. A. Wullaert, Met. Trans., 10A, Oct. 1979, pp. 1557-1570.

60. Shih, C. F., M. D. German, and V. Kumar, Int. J. Press. Vessels and Piping, 9, 1981, pp. 159-196.

61. Lee, S., L. Majno, and R. J. Asaro, Met. Trans., 16A, Sept. 1985, pp. 1633-1648.

62. Schwalbe, K.-H., Eng. Fract. Mech., 9, 1977, pp. 795-832.

63. Yermolenko, A. S., V. I. Zel'Dovich, and Ye. S. Samoylova, Fiz. Metal. Metalloved., 29, no. 2, 1970, pp. 256-264.

64. Rice, J. R. and M. A. Johnson, Inelastic Behavior of Solids, M. F. Kanninen, W. F. Adler, A. R. Rosenfield, R. J. Jaffee, eds., McGraw-Hill, 1969, pp. 641-671.

65. Tracey, D. M., J. Eng. Mat. Tech., ASME, 98, 1976, p. 146.

Table 1.
Alloy Compositions

	Cr	Ni	Mn	Si	C	N	O	P	S	Cu	Mo	Ti	V
304L1	18.90	8.29	1.84	0.33	0.019	0.087	0.011	0.024	0.015	0.33	0.43	<0.006	0.08
304L2	18.48	8.72	1.70	0.36	0.021	0.085	0.007	0.020	0.008	0.27	0.26	<0.005	0.07
304	18.62	8.11	1.52	0.26	0.039	0.089	0.004	0.023	<0.005	0.29	0.30	<0.005	0.06
310S	24.66	19.11	1.84	0.52	0.025	0.062	0.010	0.024	0.012	0.19	0.41	0.02	0.08

Table 2. 4.2 K tensile properties.

	σ_y [MPa]	σ_u [MPa]	total elongation
304L	555	1328	37
993 K-rolled 304L	536	1677	50
293 K-rolled 304L	994	1826	45
77 K-rolled 304L	2144	---	8
304	600	1340	37
310S	772	1220	68

Table 3. RMS elevations of the fracture surfaces in μm.

	304 LT	304L	RT 304L	993 K 304L	77 K 304L	310S
0 T	30	14	68	39	44	39
8T	35	36	46	45	53	61

Table 4. Line length of crack profiles normalized to the projected line length.

	304 LT	304L	RT 304L	993 K 304L	77 K 304L	310S
0 T	1.07	1.07	1.13	1.10	1.13	1.12
8 T	1.11	1.12	1.13	1.12	1.13	1.12

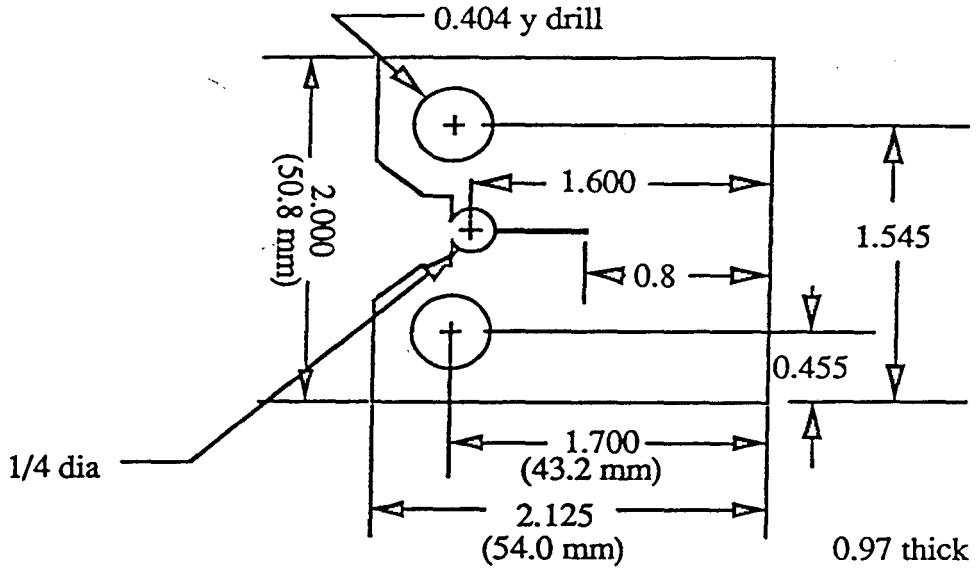

(a)

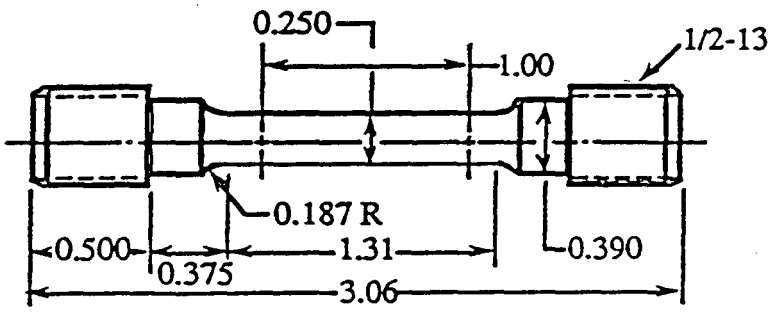

(b)

Figure 1. Configurations of (a) CT specimen and (b) tensile specimen.

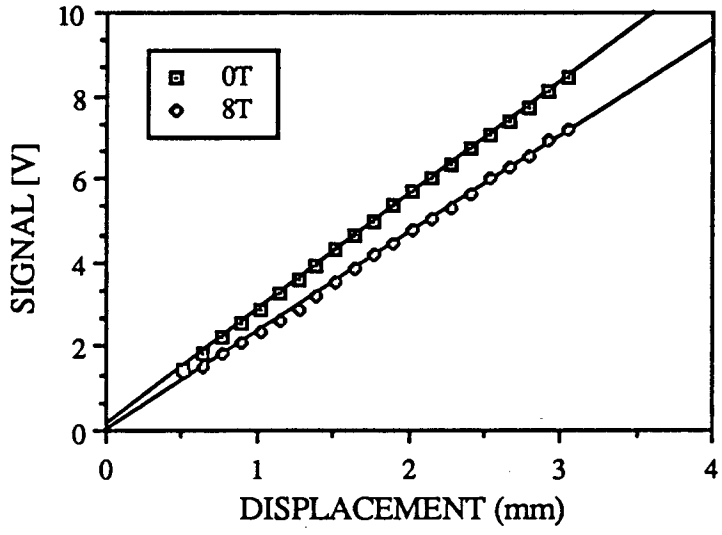

Figure 2. Typical displacement gage response change on application of an 8 T magnetic field at 4.2 K.

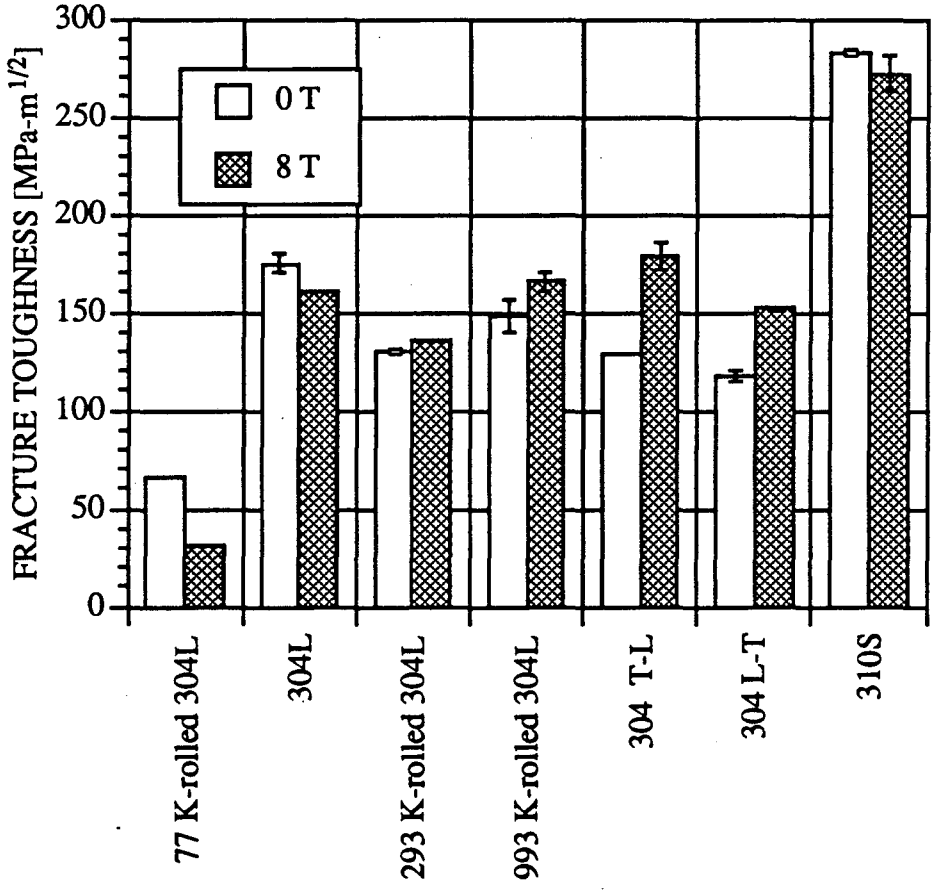

Figure 3. Fracture toughness of alloys tested at 0 T and 8 T magnetic fields. The values are $K_{IC}(J)$ except for the 77 K-rolled 304L which are from K_{IC} tests. Error bars denote spread in values. The values for 77K-rolled 304L are from one specimen in each condition only while the others are from at least two tests in each condition.

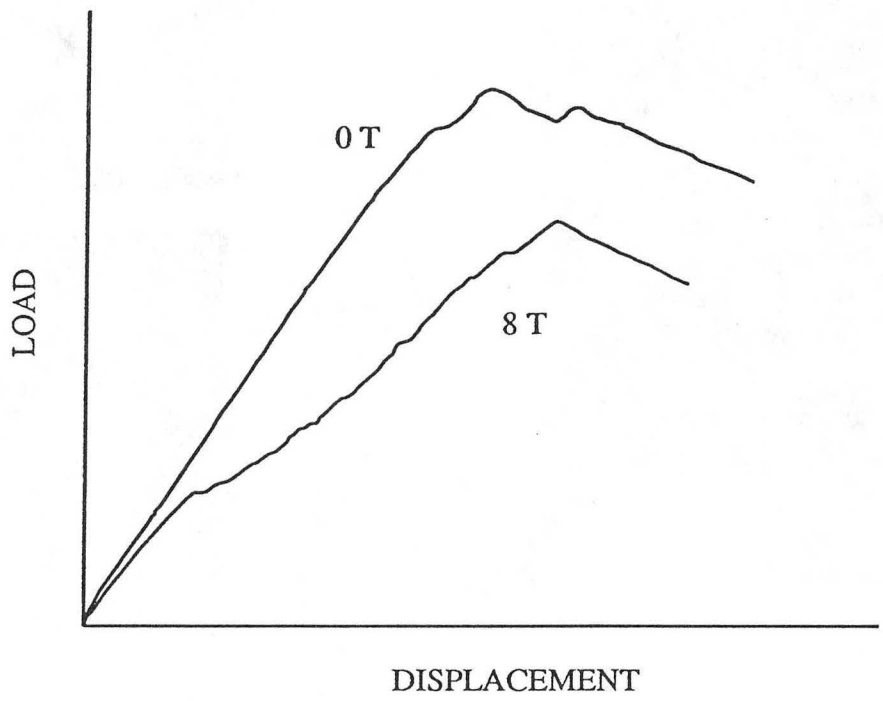

Figure 4. Raw load versus displacement curve shapes for 77 K-rolled 304L.

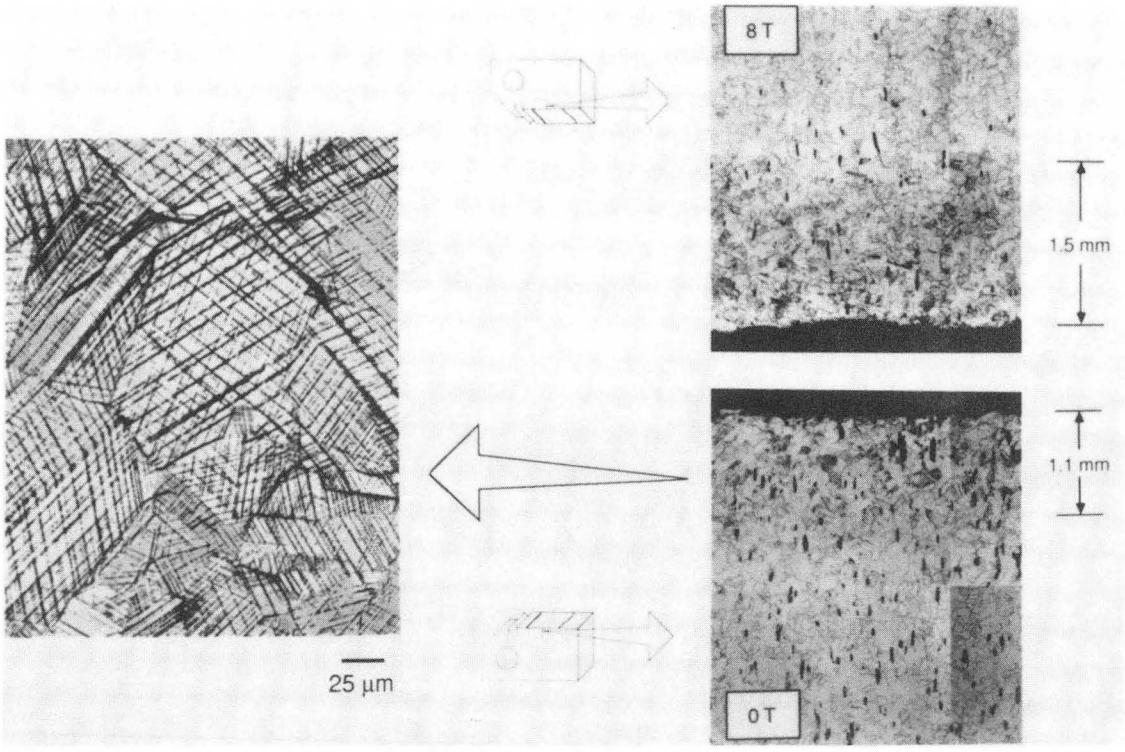

XBB 904-2832A

Figure 5. Optical fracture profiles of an AISI 304 L-T specimen tested at 4.2 K in the two magnetic field conditions. The difference in the transformation zone width as well as the martensite structures are shown.

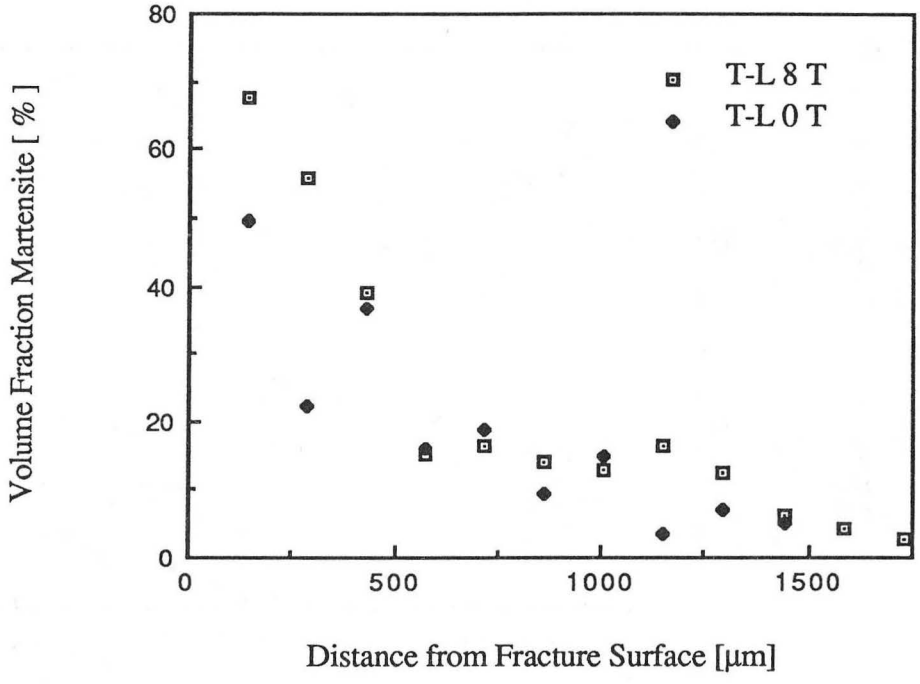

Figure 6. Martensite distribution for AISI 304 T-L CT specimens tested at 0 T and at 8 T. Measurements were made on optical fracture profiles taken from the centerplane of the CT specimens. The abscissa represents the perpendicular distance from the crack plane. The profiles are from a fully developed region of the transformed zone.

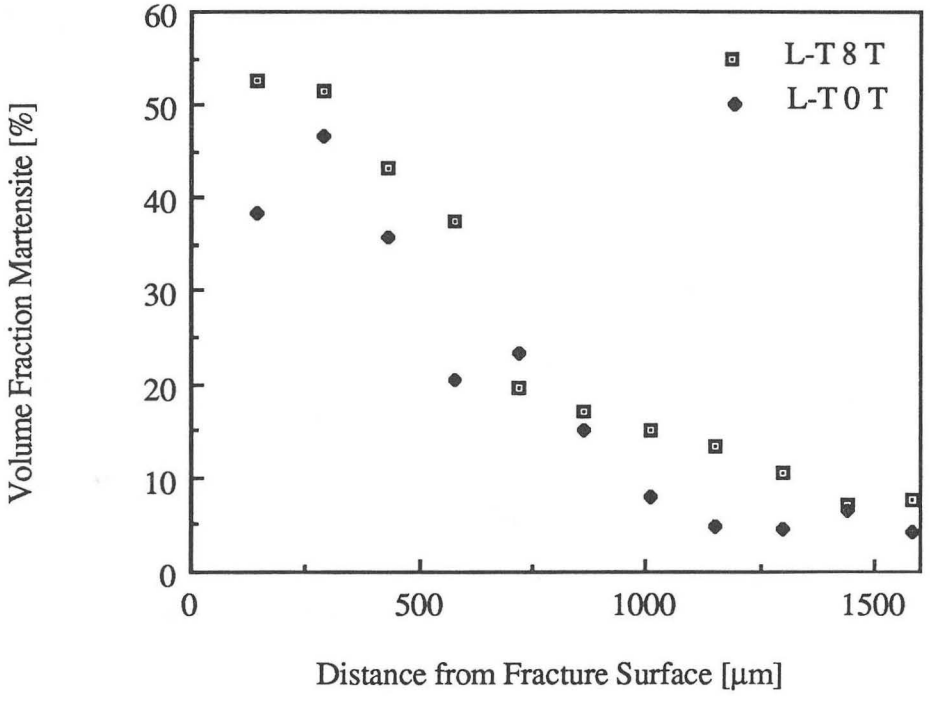

Figure 7. Martensite distribution for AISI 304 L-T CT specimens tested at 0 T and at 8 T. Measurements were made on optical fracture profiles taken from the centerplane of the CT specimens. The abscissa represents the perpendicular distance from the crack plane. The profiles are from a fully developed region of the transformed zone.

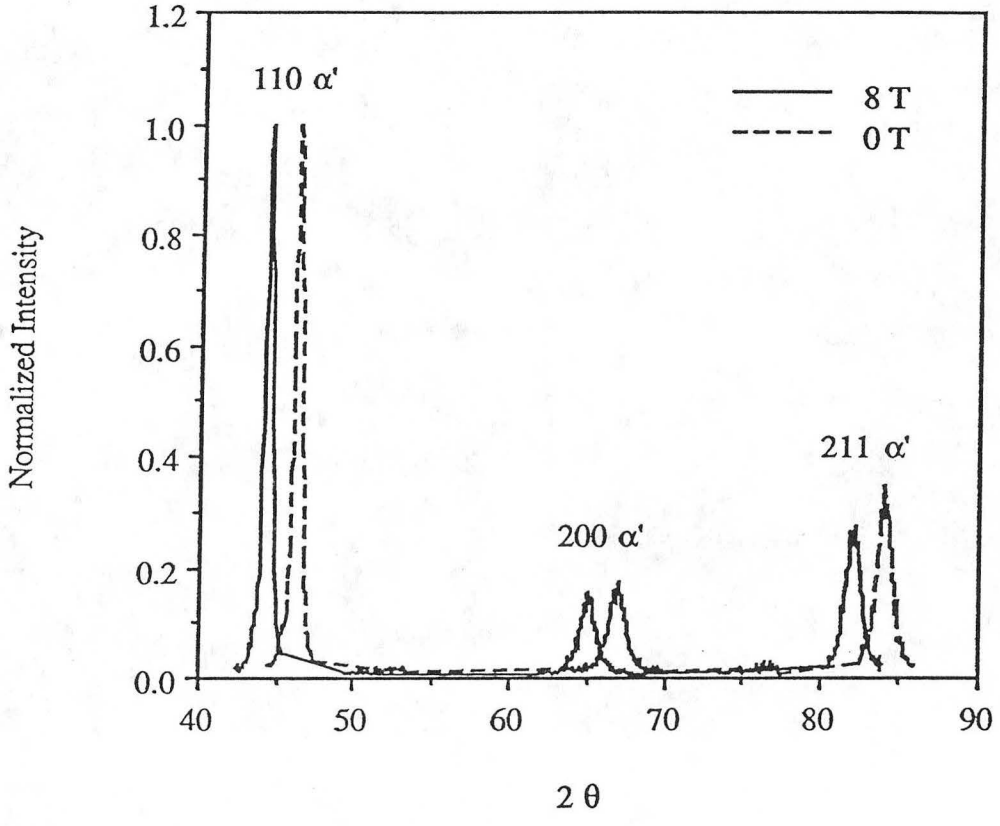

Figure 8. Normalized x-ray diffraction peaks from the 304 T-L fracture surfaces tested at 0 T and at 8 T. The 0 T peaks are offset for clarity. α' texture differences on the fracture surfaces are negligible.

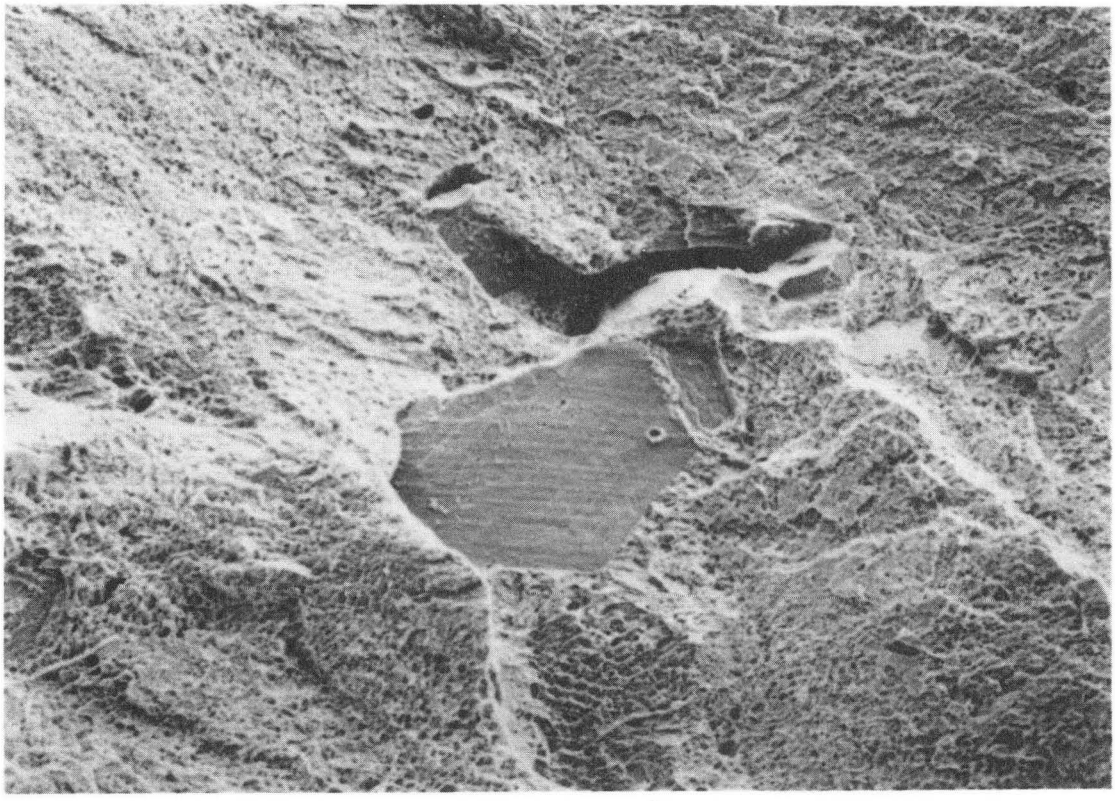

25 μm

XBB 904-2744A

Figure 9. SEM fractograph of an AISI 304 specimen tested at 4.2 K showing planar quasi-cleavage areas. There is evidence of some ductility within this region. The striations are aligned with $(111)_\gamma$.

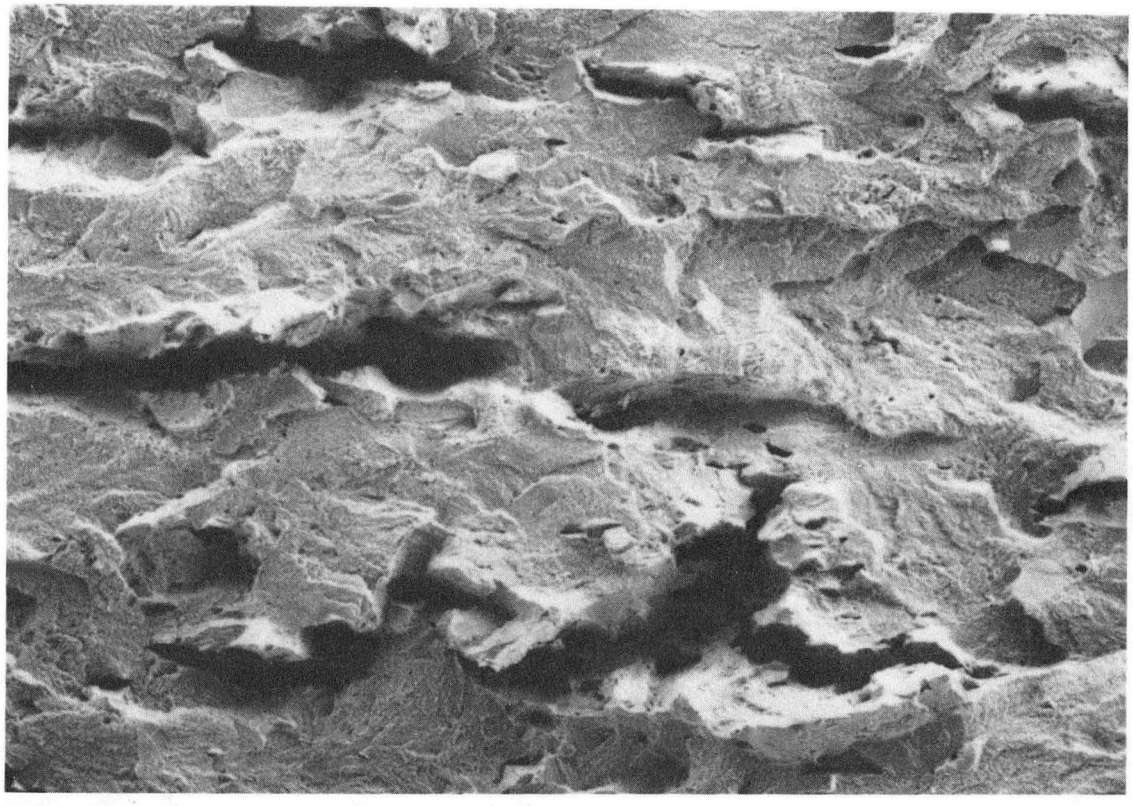

100 μm

XBB 904-2745A

Figure 10. SEM fractograph of an AISI 304 specimen tested at 4.2 K showing secondary cracking due to out-of-plane stresses. These cracks are present in all specimens tested with no obvious differences between the two magnetic field conditions. Crack propagation direction is from left to right.

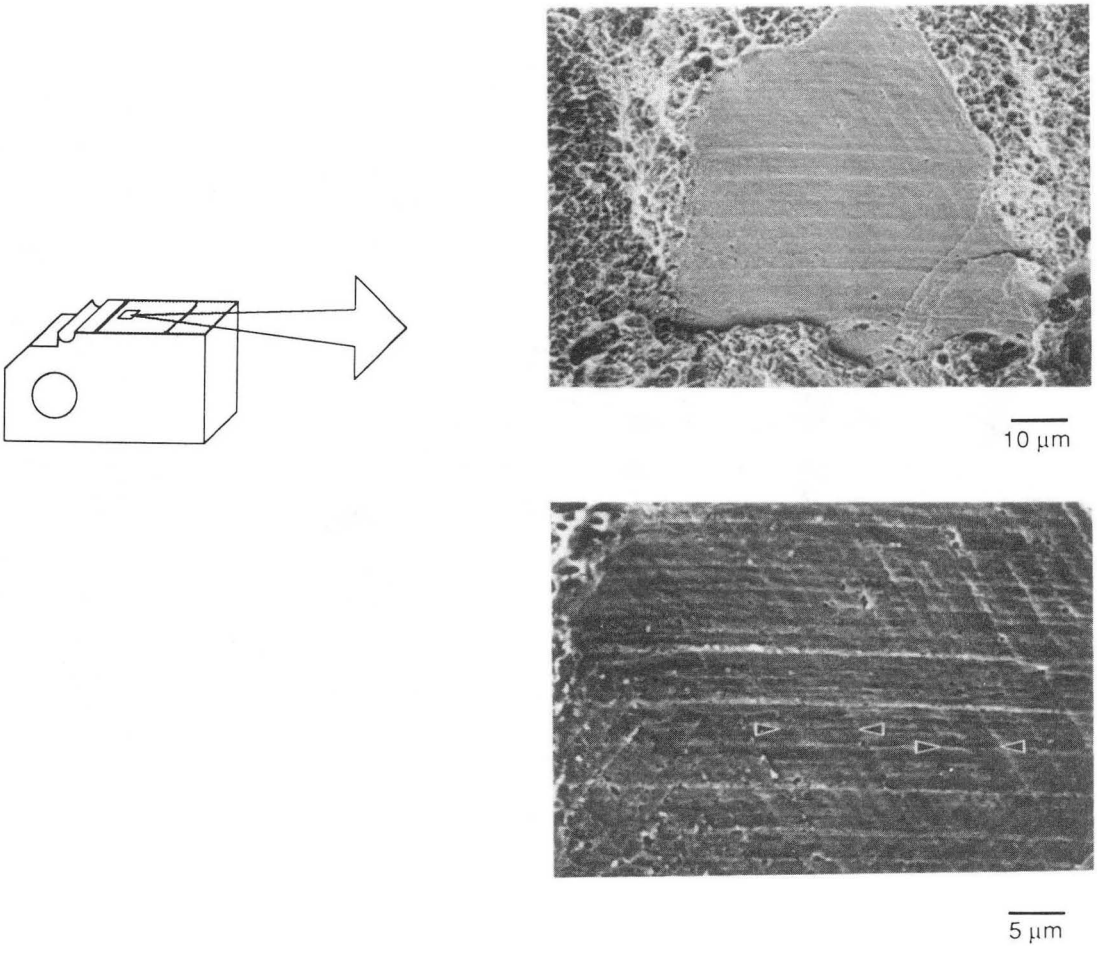

XBB 880-9706B

Figure 11. SEM fractograph of an AISI 304 specimen tested at 4.2 K showing the quasi-cleavage areas and the secondary cracks appearing between the martensite/austenite regions indicated by the arrows in the lower micrograph.

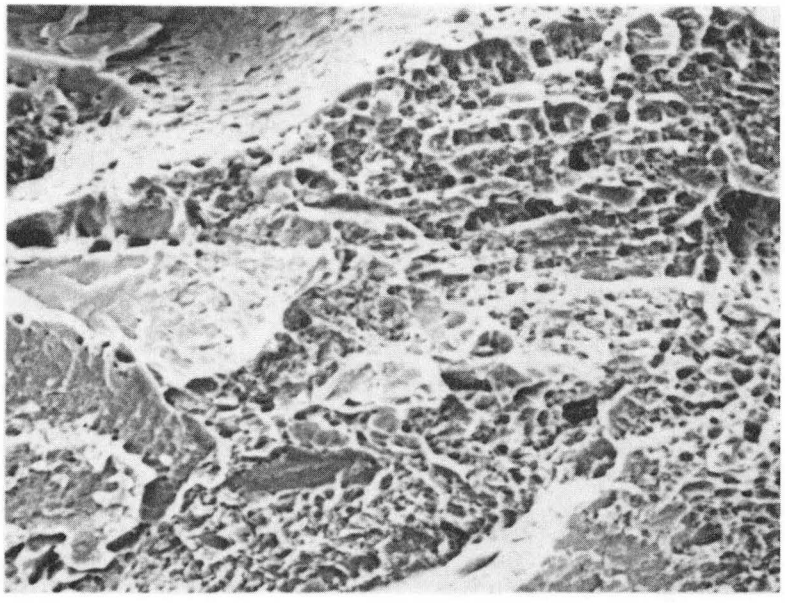

(a)

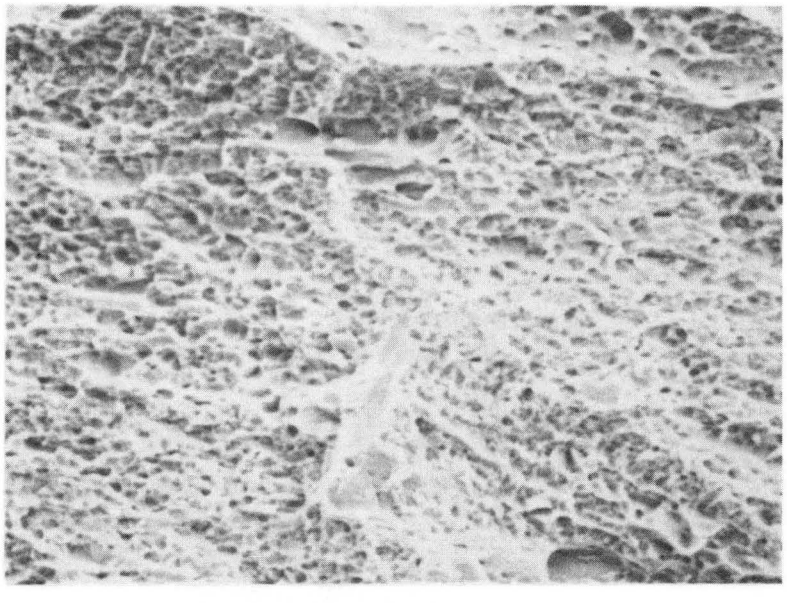

(b)

10μm

XBB 914-2853

Figure 12. SEM fractographs of AISI 304 tested at (a) 0 T and (b) 8 T near the precrack at the centerplane of the specimens. These are views of the ductile areas linking the quasi-cleavage areas and show the differences in the fracture surface morphologies. The 0 T specimen has coarser features and flatter features than the 8 T specimen. This indicates differences in the local deformation behavior.

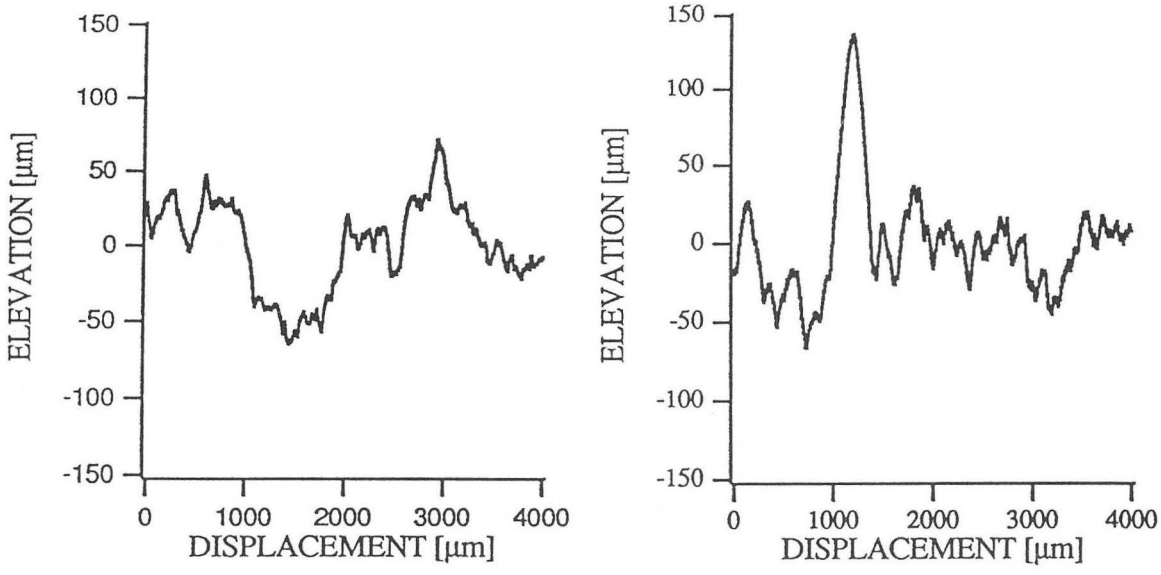

(a)

(b)

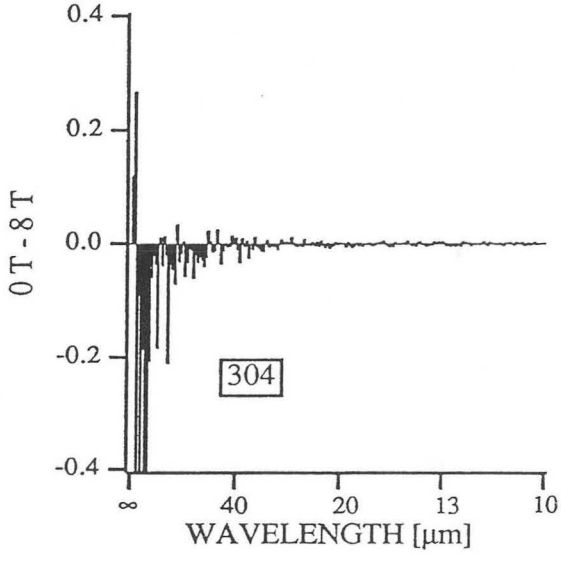

(c)

Figure 13. Fracture surface profiles of AISI 304 tested at 4.2 K in (a) 0 T and (b) 8 T magnetic fields. (c) Difference spectrum (0 T - 8 T) formed from the normalized power spectra of a and b.

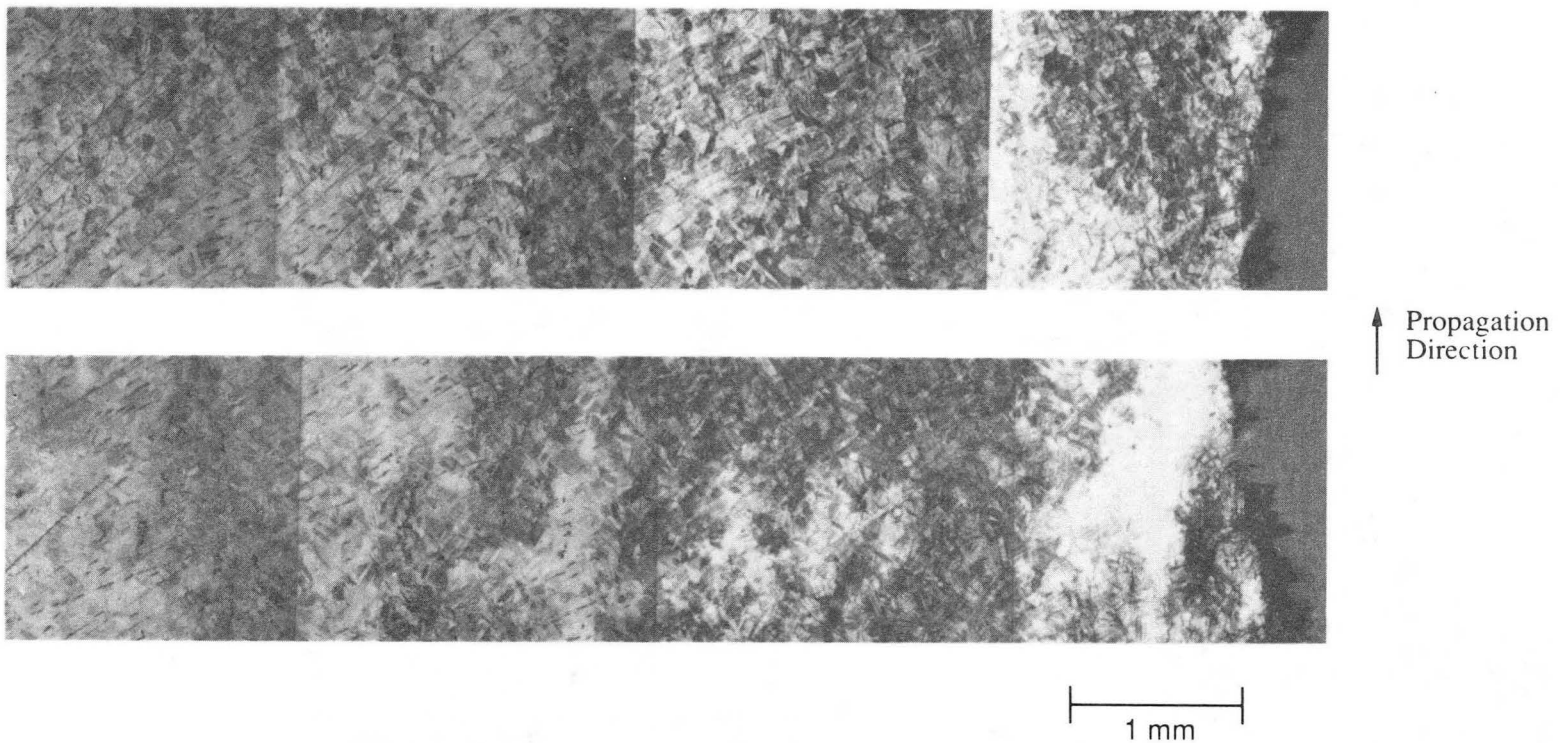

XBB 914-2526A

Figure 14. Optical fracture profiles of AISI 304L CT specimens tested in 0 T (upper) and in 8 T (lower) magnetic fields at 4.2 K. Dark areas contain martensite. The fracture surface is on the right. Propagation direction is from bottom to top.

(a)

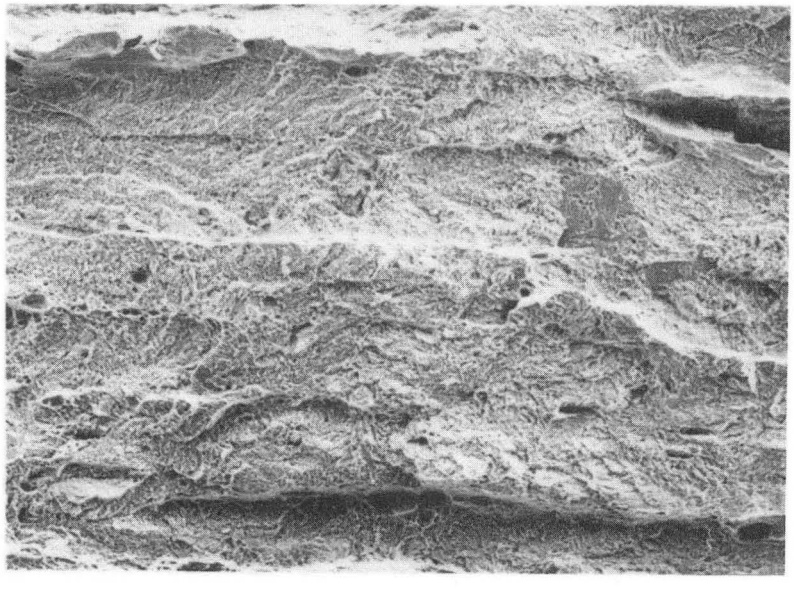

(b)

40μm

Figure 15. SEM fractographs of AISI 304L tested at (a) 0 T and (b) 8 T near the precrack at the centerplane of the specimens. The crack propagates from left to right.

XBB 914-2854

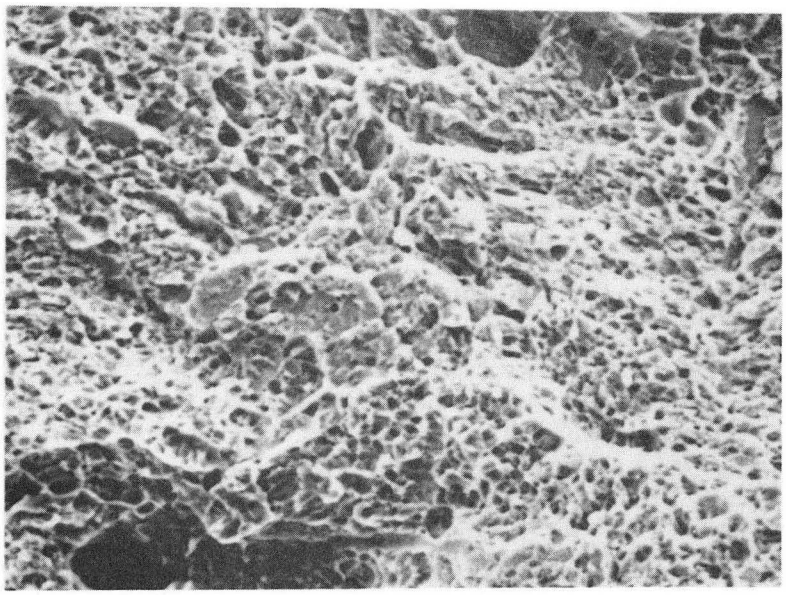

(a)

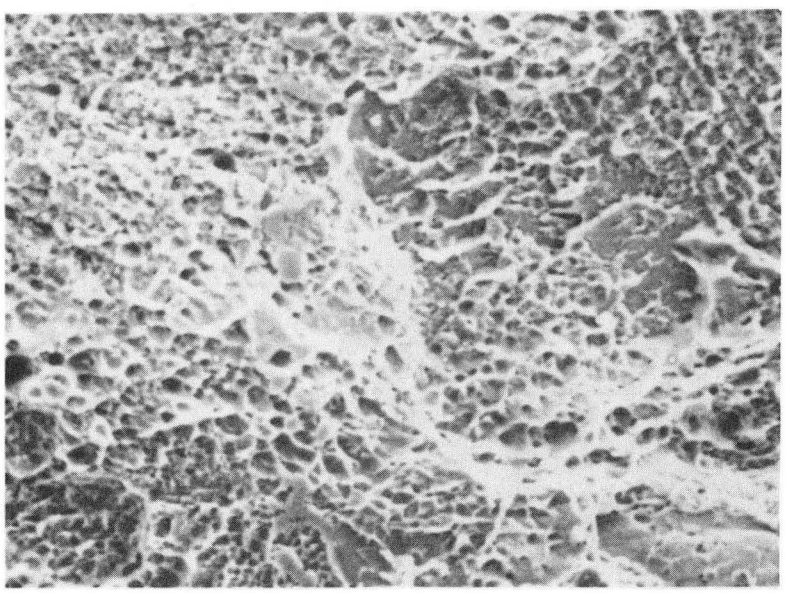

(b)

10μm

XBB 914-2855

Figure 16. SEM fractographs of AISI 304L tested at (a) 0 T and (b) 8 T near the precrack at the centerplane of the specimens. These are views of the ductile areas linking the quasi-cleavage areas and show the differences in the fracture surface morphologies. The 8 T specimen has coarser features and flatter features than the 0 T specimen. This indicates differences in the local deformation behavior.

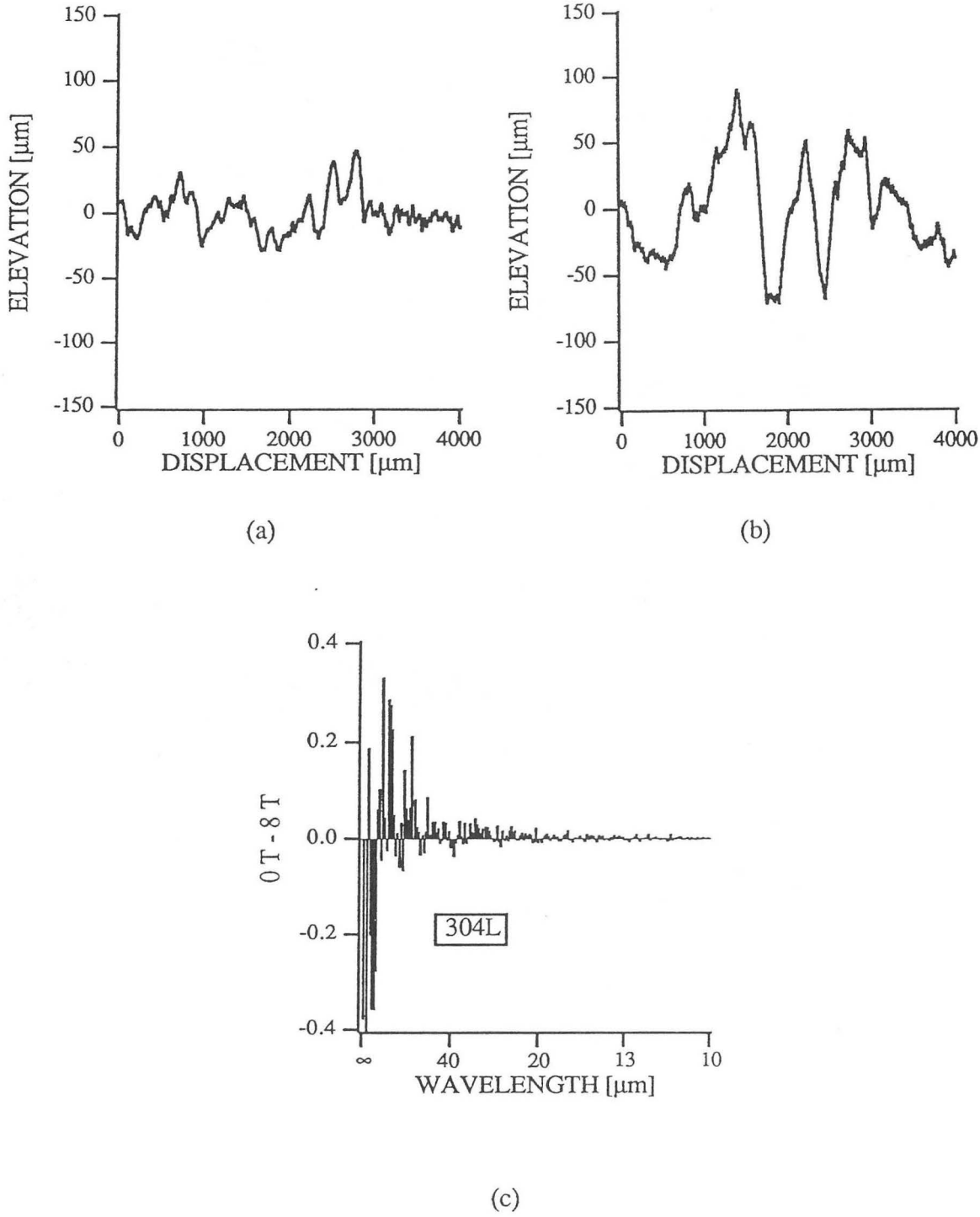

Figure 17. Fracture surface profiles of AISI 304L tested at 4.2 K in (a) 0 T and (b) 8 T magnetic fields. (c) Difference spectrum (0 T - 8 T) formed from the normalized power spectra of a and b.

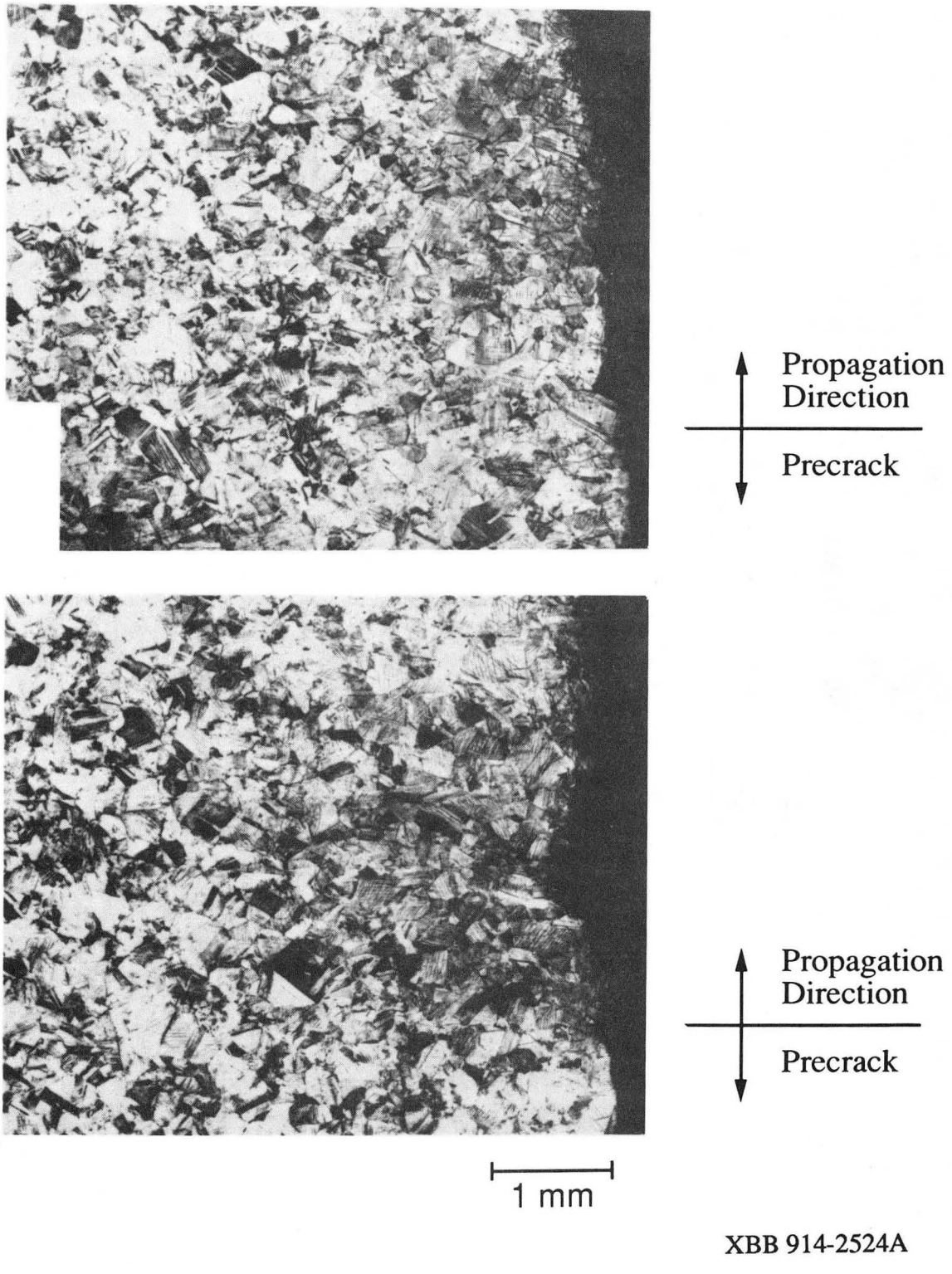

Figure 18. Optical fracture profiles for 293 K-rolled AISI 304L CT specimens tested in 0 T (upper) and 8 T (lower) magnetic fields at 4.2 K. Dark areas contain martensite. The finer α' structures near the fracture surface is formed in situ during the tests. The fracture surface is on the right.

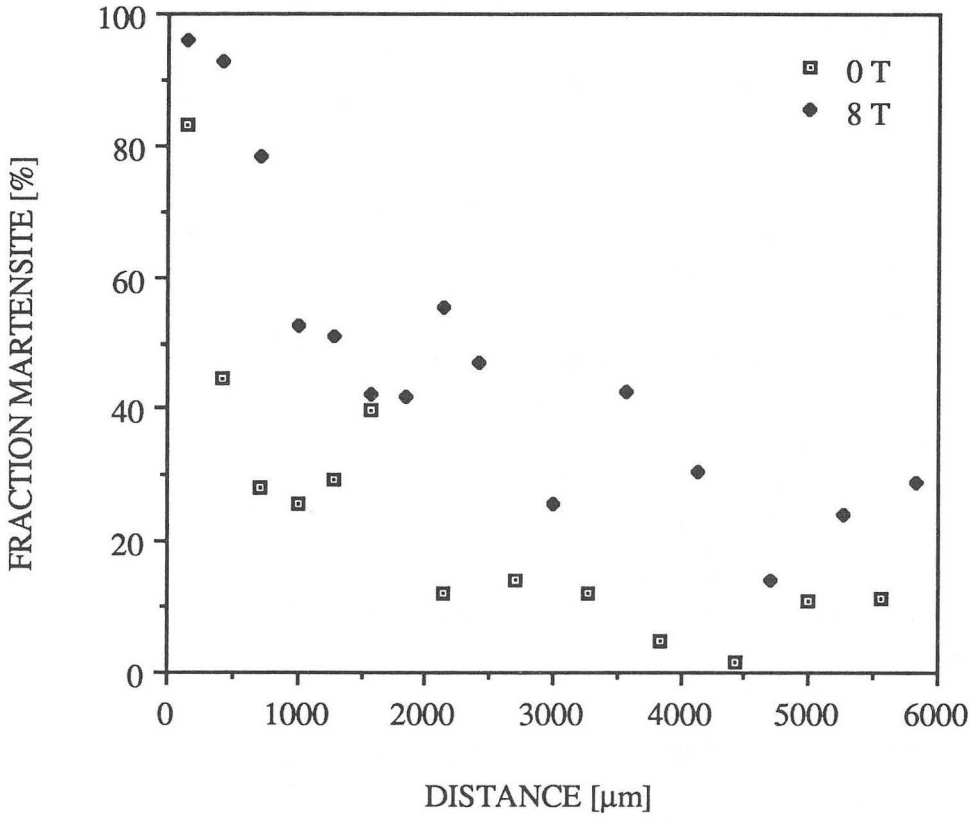

Figure 19. Martensite distribution for 293 K-rolled 304L.

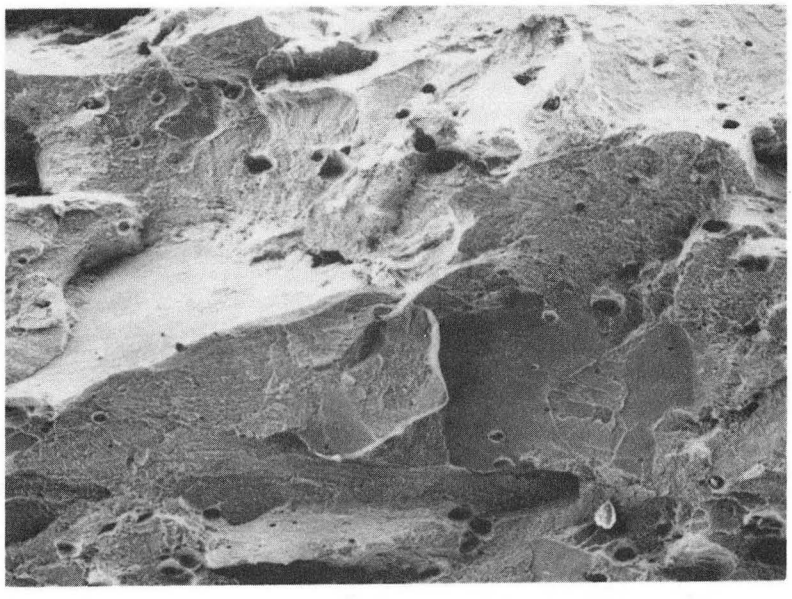

(a)

(b)

70μm

Figure 20. SEM fractographs of 293 K-rolled AISI 304L tested at (a) 0 T and (b) 8T near the precrack at the centerplane of the specimens. The crack propagates from left to right.

XBB 914-2856

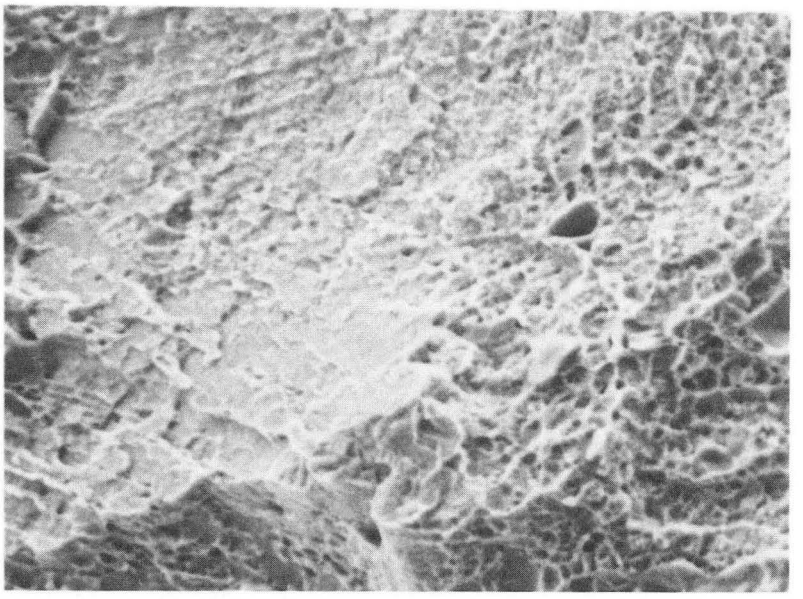

(a)

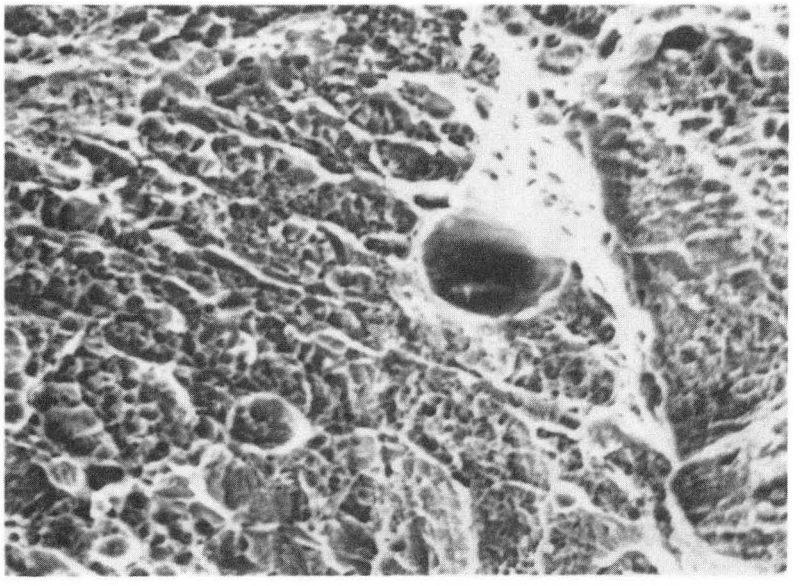

(b)

10μm

XBB 914-2857

Figure 21. SEM fractographs of 293 K-rolled AISI 304L tested at (a) 0 T and (b) 8 T near the precrack at the centerplane of the specimens. These are views of the ductile areas linking the quasi-cleavage areas and show the differences in the fracture surface morphologies. The 0 T specimen has coarser features and flatter features than the 8 T specimen. This indicates differences in the local deformation behavior.

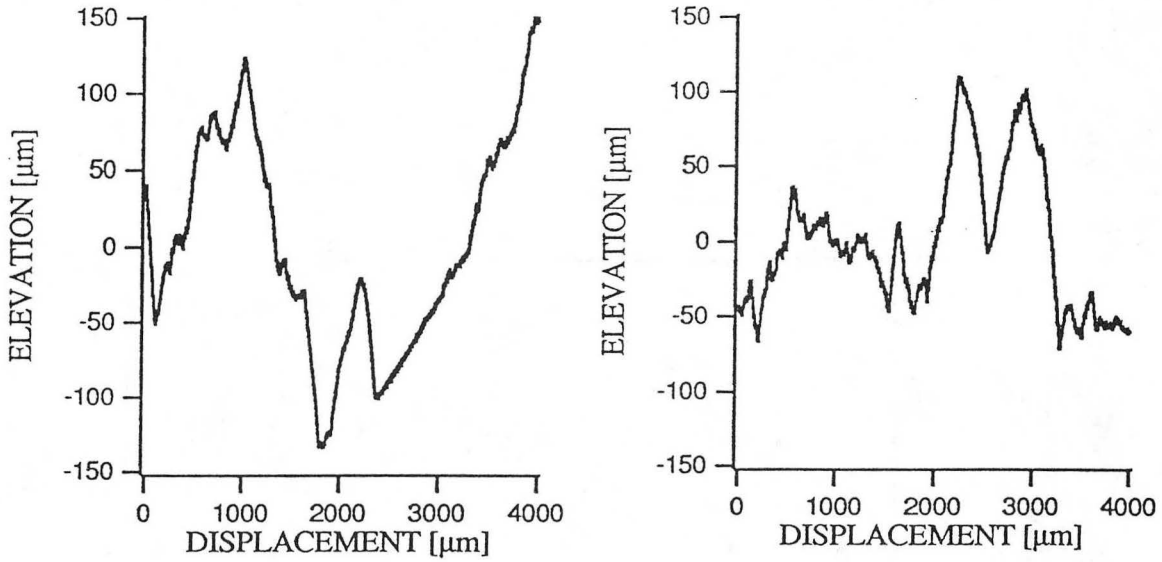

(a)

(b)

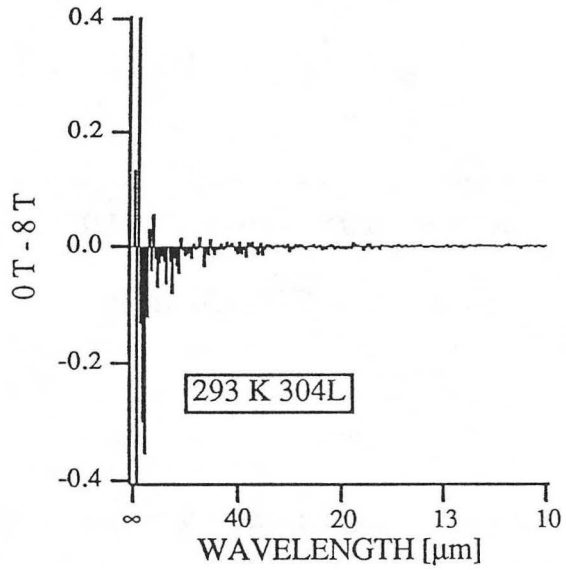

(c)

Figure 22. Fracture surface profiles of 293 K-rolled 304L tested at 4.2 K in (a) 0 T and (b) 8 T magnetic fields. (c) Difference spectrum (0 T - 8 T) formed from the normalized power spectra of a and b.

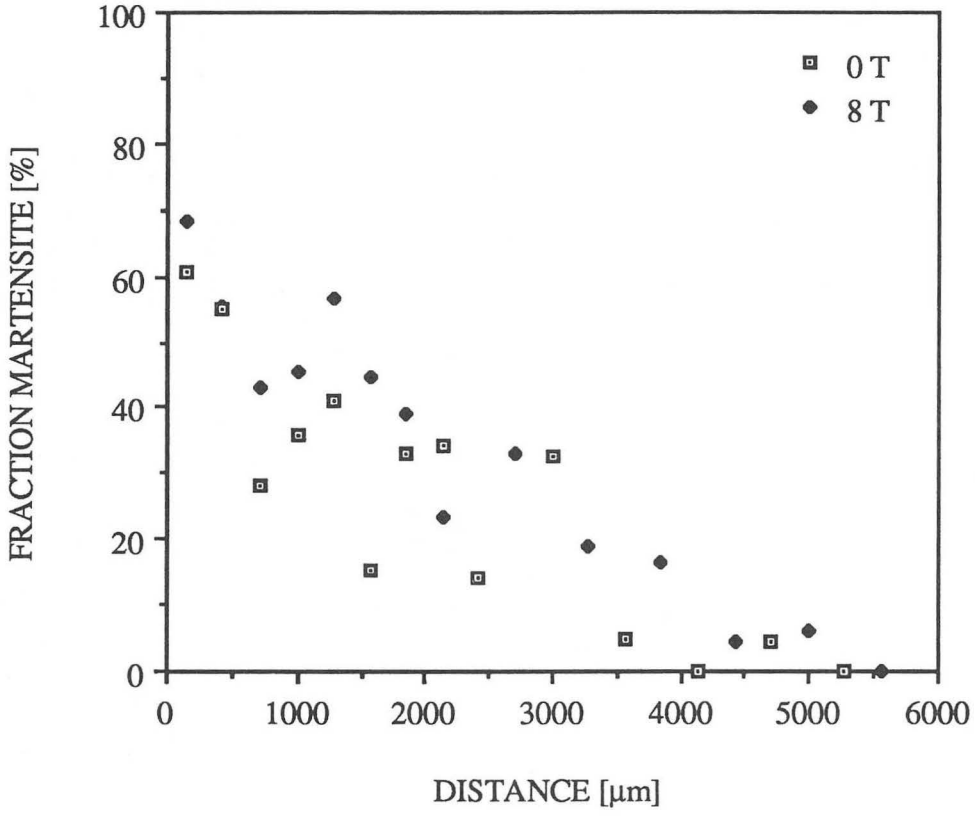

Figure 23. Martensite distribution for 993 K-rolled 304L.

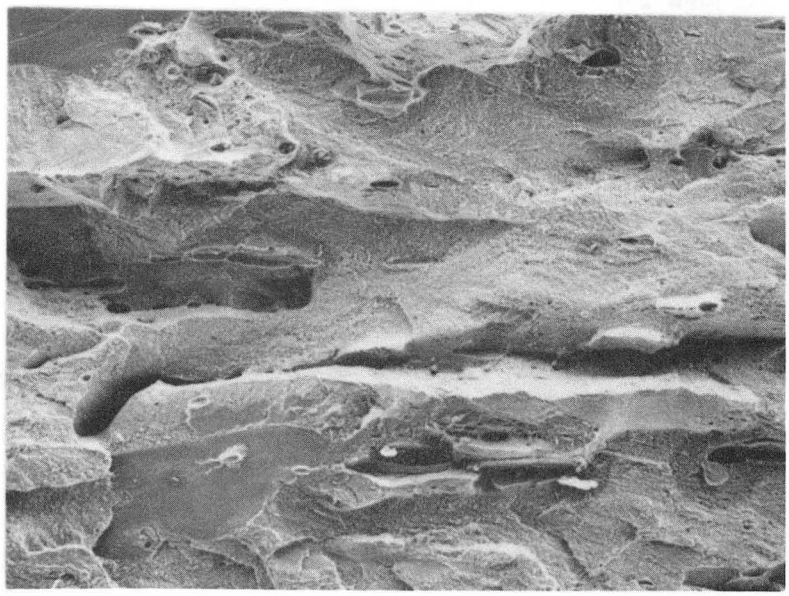

(a)

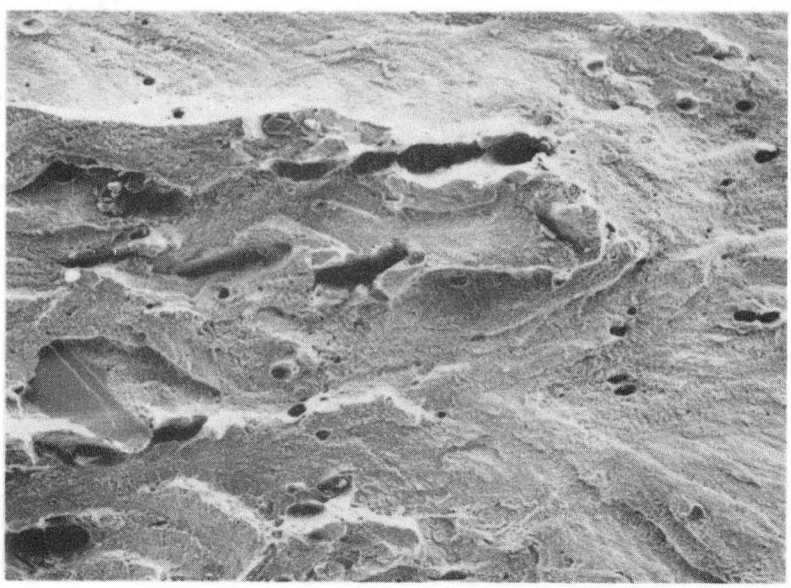

(b)

65μm

Figure 24. SEM fractographs of 993 K-rolled AISI 304L tested at (a) 0 T and (b) 8T near the precrack at the centerplane of the specimens. The crack propagates from left to right.

XBB 914-2858

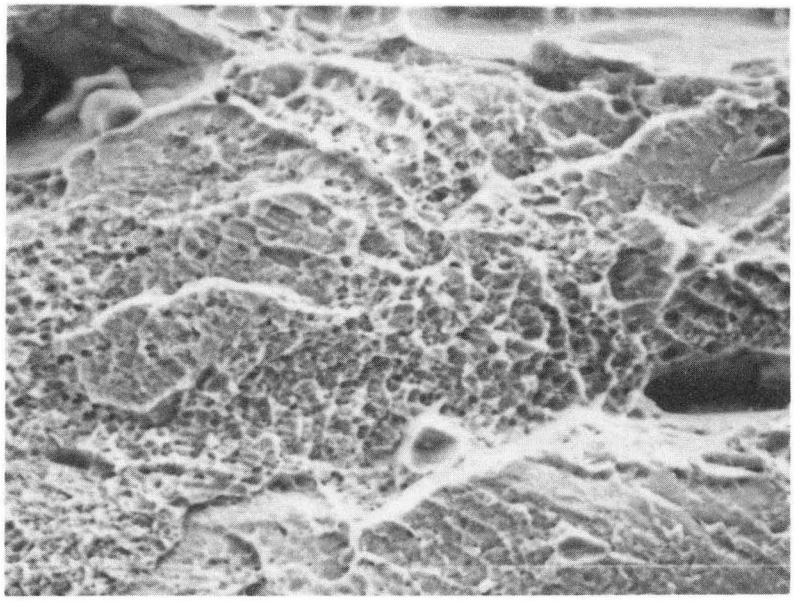

(a)

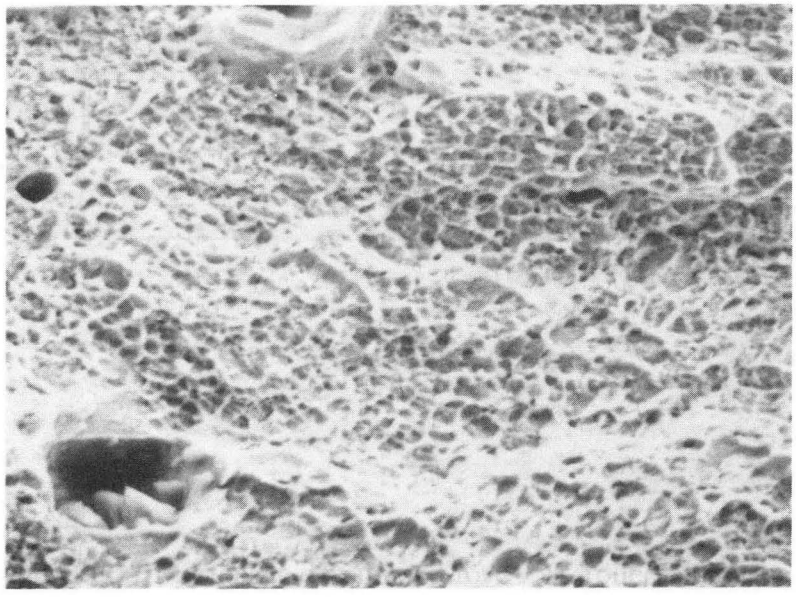

(b)

10μm

XBB 914-2859

Figure 25. SEM fractographs of 993 K-rolled AISI 304L tested at (a) 0 T and (b) 8 T near the precrack at the centerplane of the specimens. These are views of the ductile areas linking the quasi-cleavage areas and show the differences in the fracture surface morphologies. The 0 T specimen has coarser features and flatter features than the 8 T specimen. This indicates differences in the local deformation behavior.

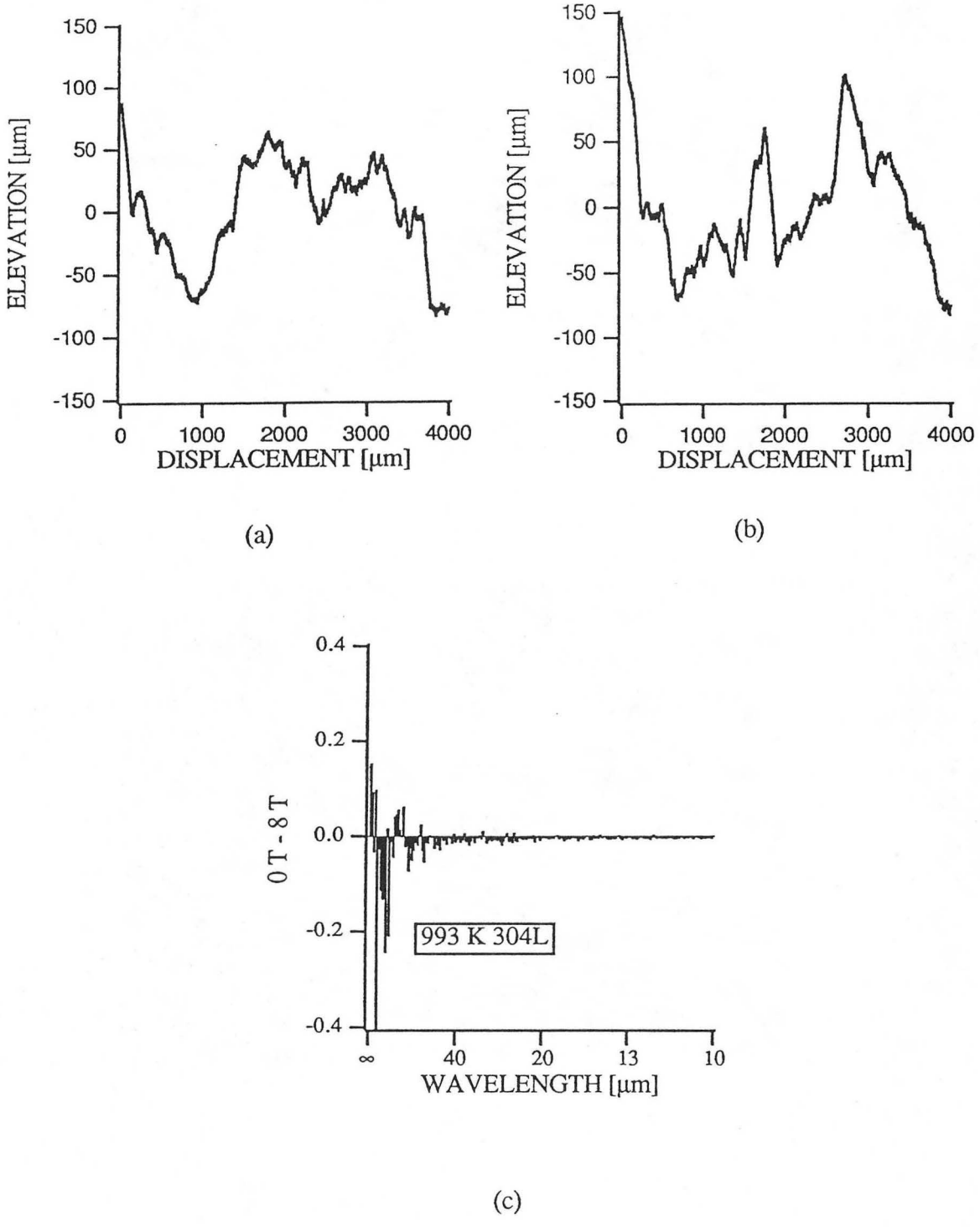

Figure 26. Fracture surface profiles of 993 K-rolled 304L tested at 4.2 K in (a) 0 T and (b) 8 T magnetic fields. (c) Difference spectrum (0 T - 8 T) formed from the normalized power spectra of a and b.

(a)

(b)

80μm

XBB 914-2860

Figure 27. SEM fractographs of 77 K-rolled AISI 304L tested at (a) 0 T and (b) 8T near the precrack at the centerplane of the specimens. The crack propagates from left to right.

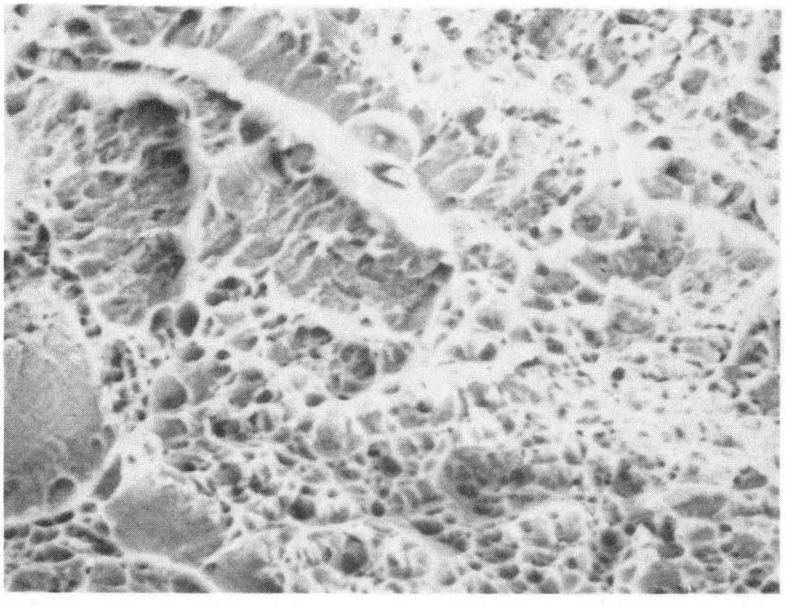

(a)

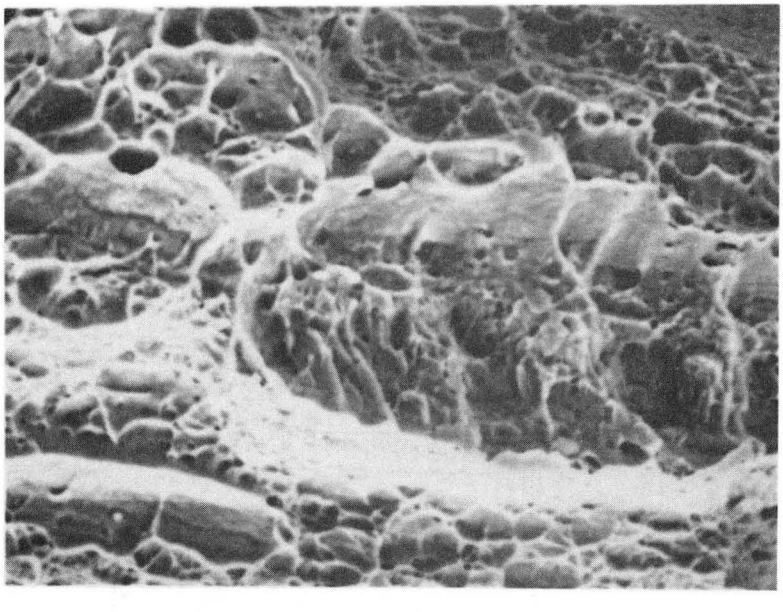

(b)

10μm

XBB 914-2861

Figure 28. SEM fractographs of 77 K-rolled AISI 304L tested at (a) 0 T and (b) 8 T near the precrack at the centerplane of the specimens. These are views of the ductile areas linking the quasi-cleavage areas and show the differences in the fracture surface morphologies. The 8 T specimen has coarser and flatter features than the 0 T specimen. This indicates differences in the local deformation behavior.

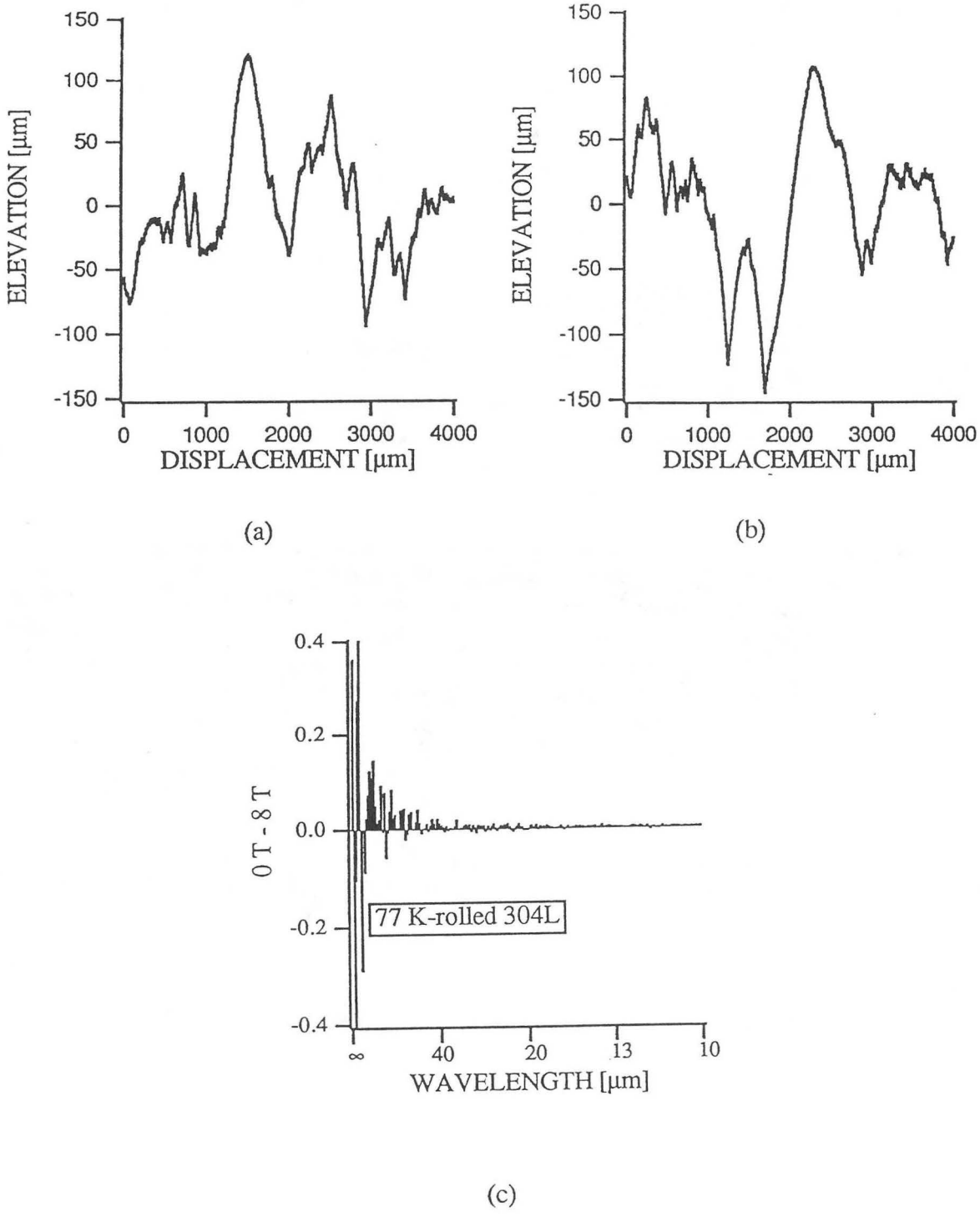

Figure 29. Fracture surface profiles of 77 K-rolled 304L tested at 4.2 K in (a) 0 T and (b) 8 T magnetic fields. (c) Difference spectrum (0 T - 8 T) formed from the normalized power spectra of a and b.

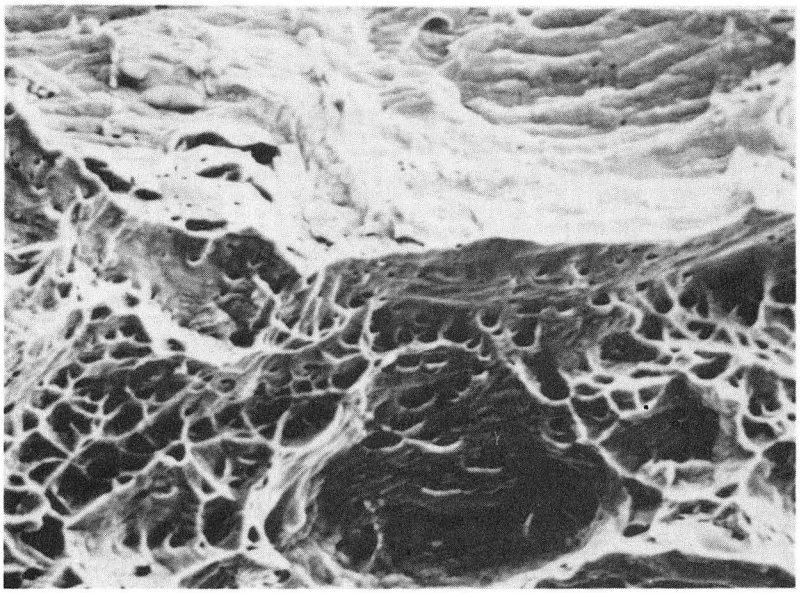

(a)

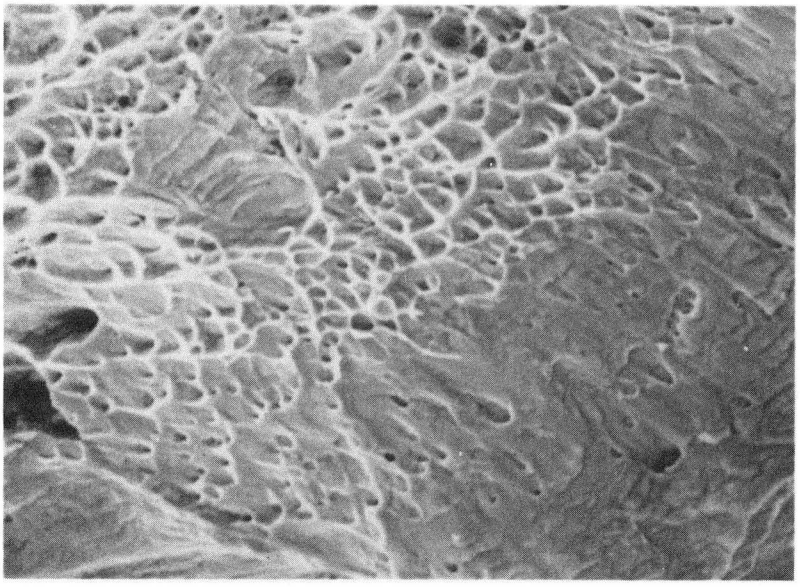

(b)

10μm

XBB 914-2862

Figure 30. SEM fractographs of AISI 310S tested at (a) 0 T and (b) 8 T near the precrack at the centerplane of the specimens. The crack propagates from left to right.

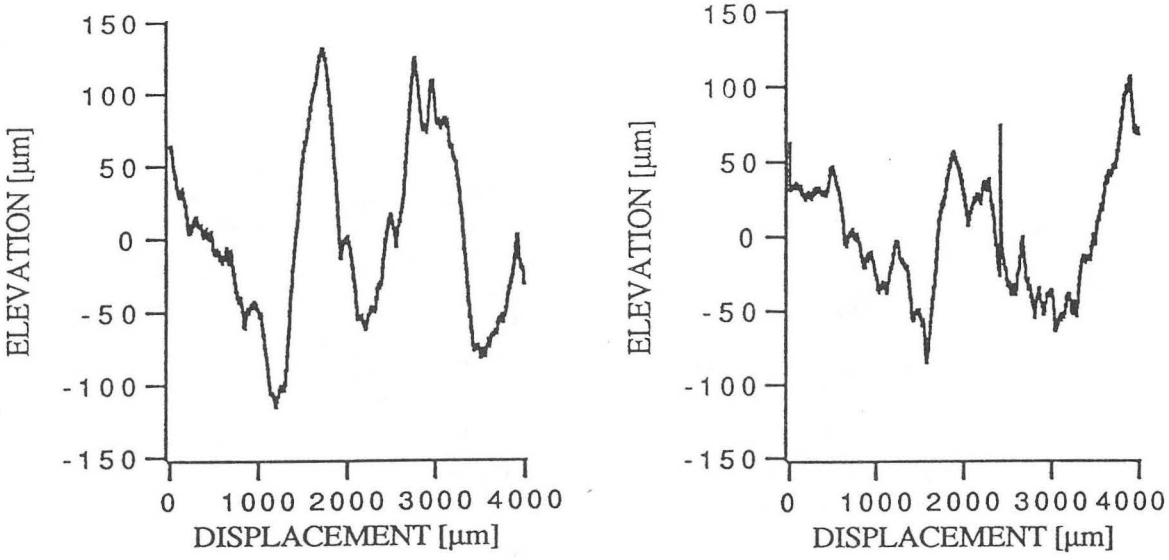

(a)

(b)

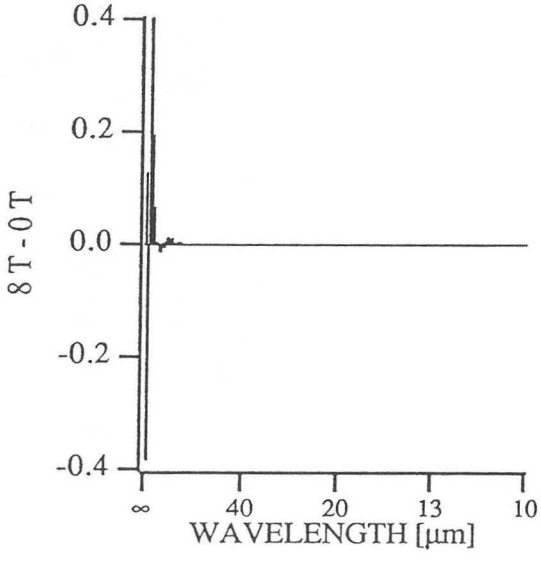

(c)

Figure 31. Fracture surface profiles of AISI 310S tested at 4.2 K in (a) 0 T and (b) 8 T magnetic fields. (c) Difference spectrum (8 T - 0 T) formed from the normalized power spectra of a and b.

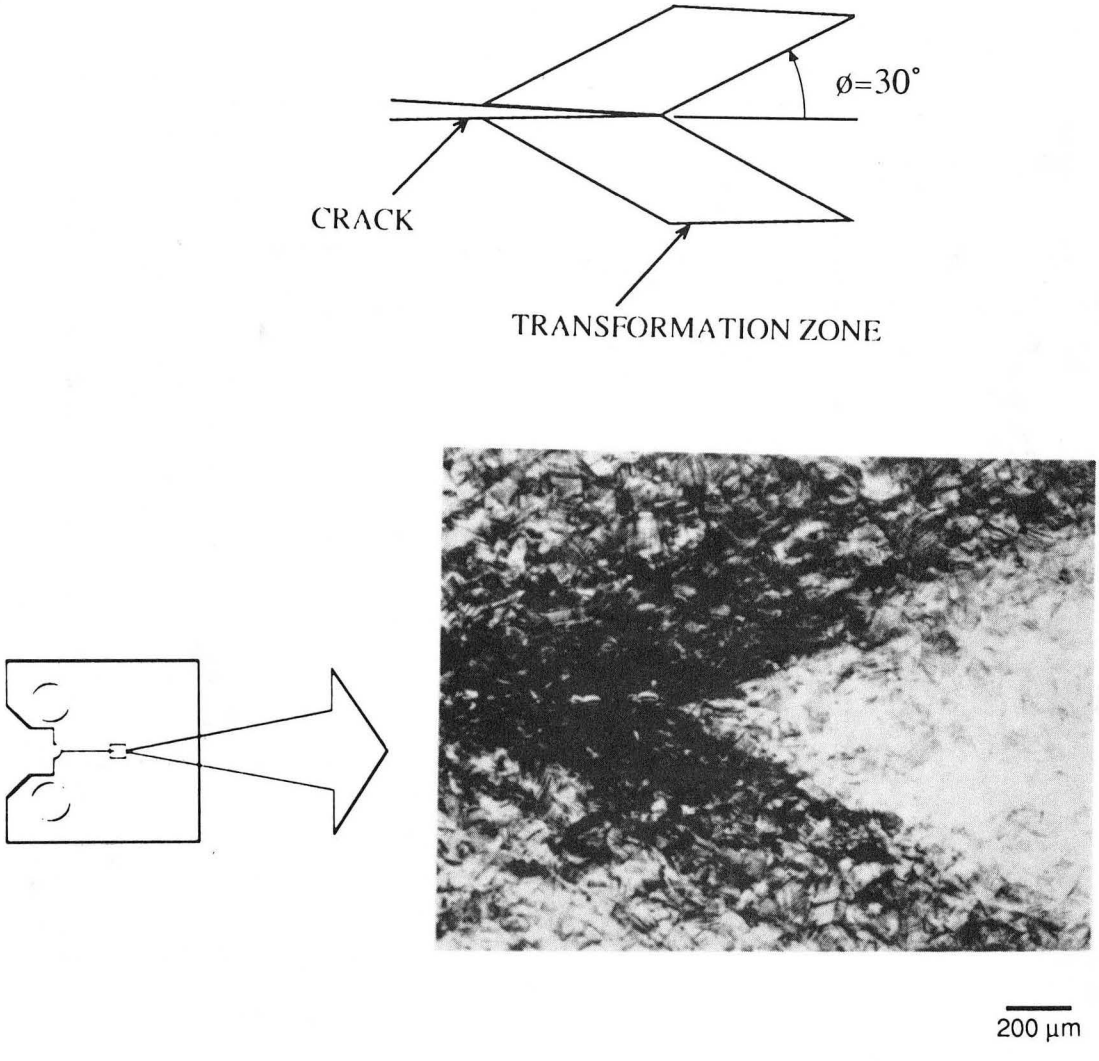

XBB 880-9765B

Figure 32. Optical micrograph of the transformation zone at the crack tip. Dark region contains martensite. Note the small amount of martensite present ahead of the crack. This is from an AISI 304 specimen. Above is the zone shape used in the calculations of the transformation dilatation contribution to the fracture toughness.

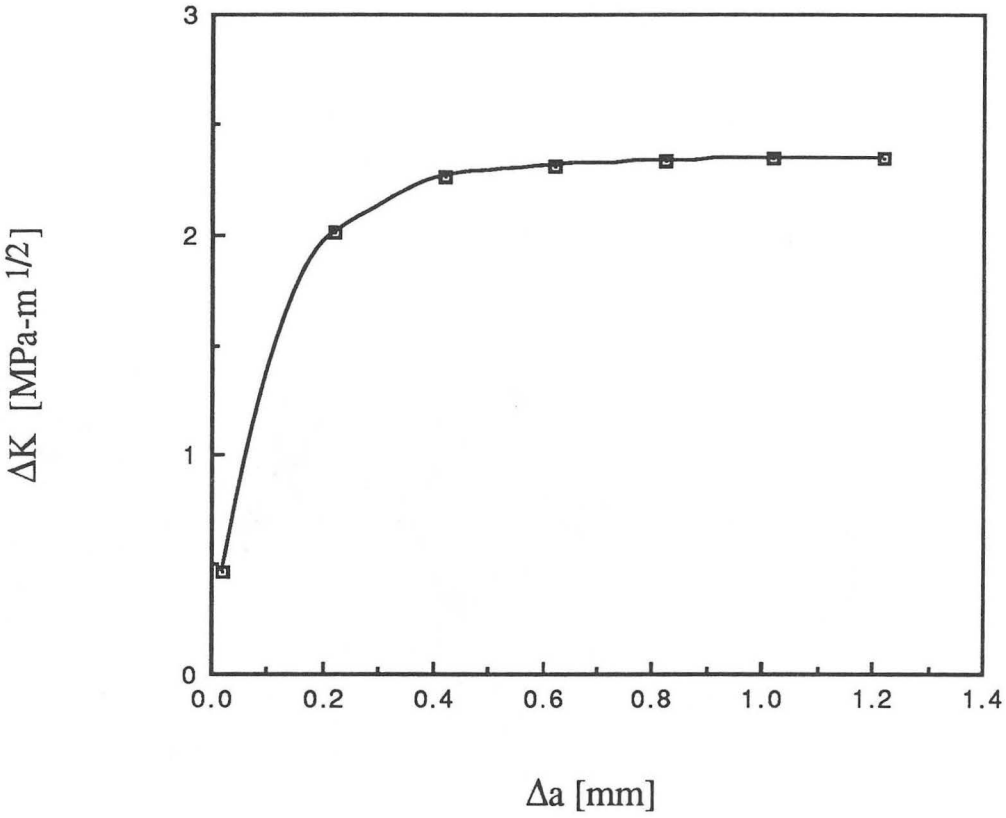

Figure 33. Calculated decrease in K_I due to transformation strain as a function of crack growth.

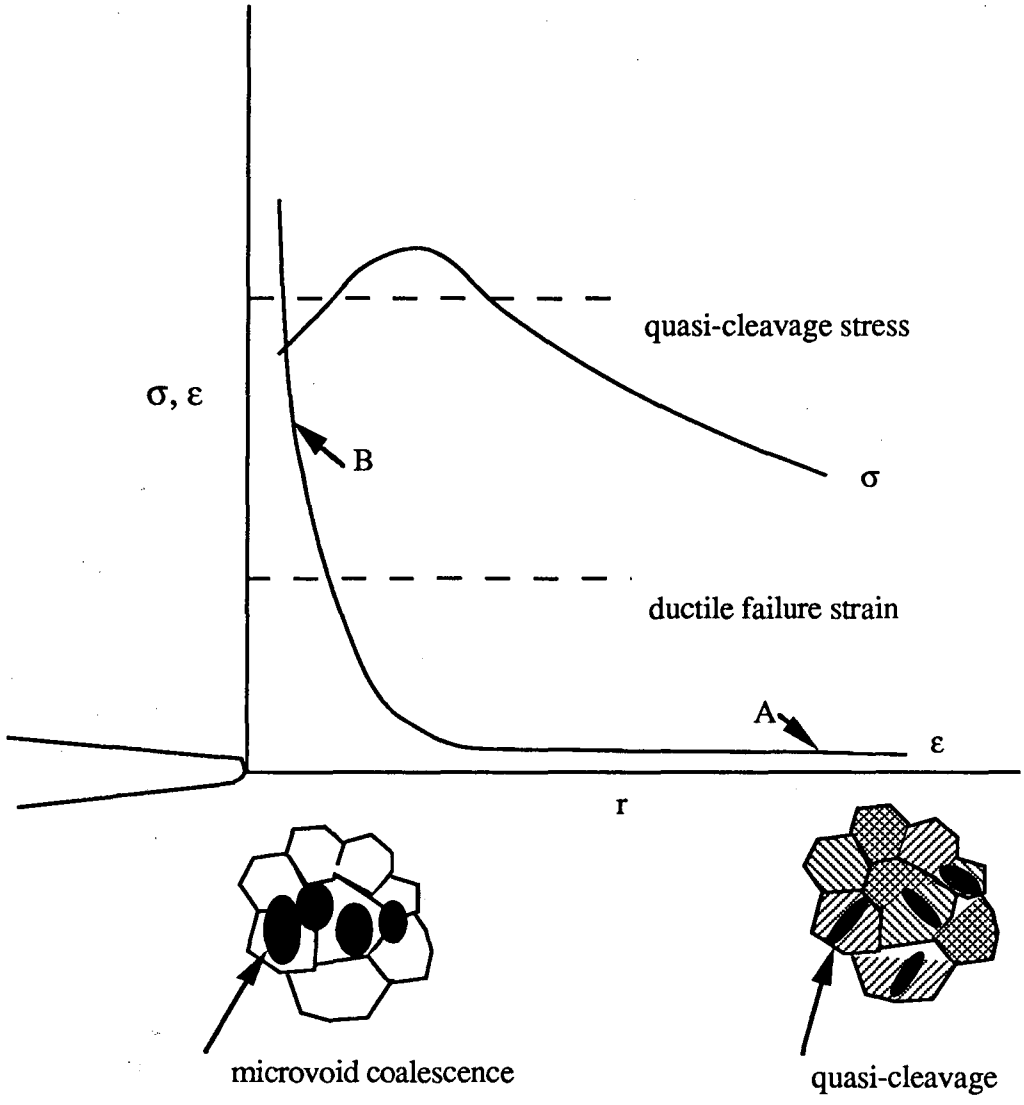

Figure 34. Schematic illustration of the stress and strain distributions ahead of a blunted crack. If the transformation initiates at A and is extensive before reaching the critical fracture stress, quasi-cleavage through α' regions is enhanced and toughness is lowered. If transformation occurs at B, microvoid nucleation and growth occurs before formation of the α' and toughness is raised.

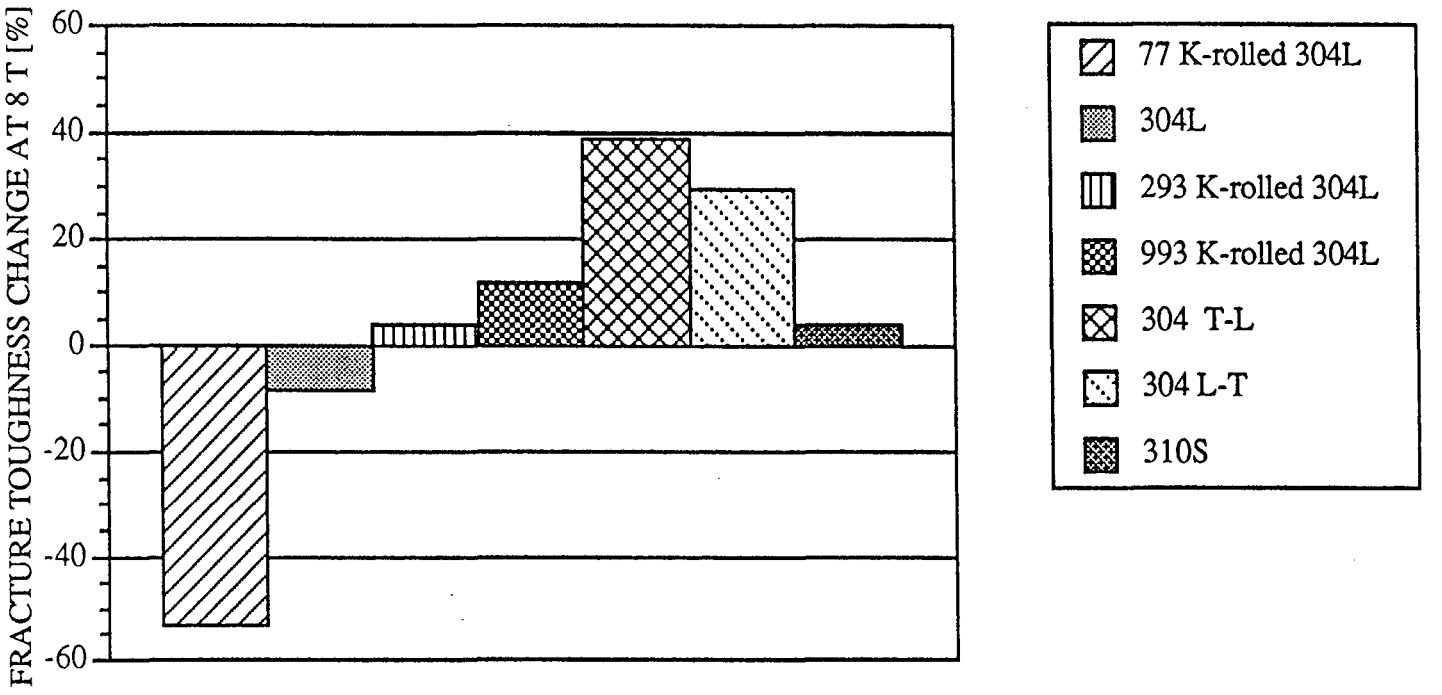

Figure 35. Percentage change in fracture toughness in an 8 T magnetic field plotted approximately in order of alloy stability.

LAWRENCE BERKELEY LABORATORY
CENTER FOR ADVANCED MATERIALS
1 CYCLOTRON ROAD
BERKELEY, CALIFORNIA 94720